EFFECTS OF ION REFLECTION ON THE COLLECTOR AND SOURCE SHEATHS OF A FINITE ION TEMPERATURE PLASMA

by

L. A. Schwager

Memorandum No. UCB/ERL M88/25

13 April 1988

COVER PAGE

EFFECTS OF ION REFLECTION ON THE COLLECTOR AND SOURCE SHEATHS OF A FINITE ION TEMPERATURE PLASMA

by

L. A. Schwager

Memorandum No. UCB/ERL M88/25

13 April 1988

ELECTRONICS RESEARCH LABORATORY

College of Engineering
University of California, Berkeley
94720

EFFECTS OF ION REFLECTION ON THE COLLECTOR AND SOURCE SHEATHS OF A FINITE ION TEMPERATURE PLASMA

by

L. A. Schwager

Memorandum No. UCB/ERL M88/25

13 April 1988

ELECTRONICS RESEARCH LABORATORY

College of Engineering
University of California, Berkeley
94720

Table of Contents

3

Effects of Ion Reflection on the Collector and and Source Sheaths of a Finite Ion Temperature Plasma

The region between a Maxwellian plasma source and an absorbing surface which reflects a fraction of the incident ions is modeled numerically with dynamic, electrostatic particle simulation and theoretically with a static, kinetic plasma-sheath model. The fraction ζ of ions reflected is varied from 0 to 0.6 which generally increases both the potential drop from the source to the collector and the energy transported to the collector surface. Results from both models agree well when the fraction reflected is less than 0.4 for full energy transfer to reflected ions. With larger fractions and with slightly less than full reflected energy, simulations show an ion-ion two-streaming interaction which slightly reduces the collector potential drop and decreases the ion energy deposited on the collector surface relative to predictions from the static theory. According to theory, for a deuterium-tritium plasma, a collector material causing the reflected ion fraction to be $\zeta = 0.2$ with full reflected energy increases the magnitude of collector potential by 12% and the ion energy deposited by 6% over those predicted when $\zeta = 0$.

I. INTRODUCTION

A. Problem description

Near an electrically floating collector, an electrostatic sheath forms which impedes the flow of plasma electrons in order to balance ion and electron currents at the collector surface. Ions are accelerated by the potential drop through the sheath and strike the collector surface. Typically some ions backscatter directly from the surface and the remainder penetrate the collector solid and collide with collector atoms. Some fraction of these scatter back to the surface. For hydrogen plasma ions, the reflected particles can emerge as positive ions, negative ions, or neutrals.[1] Of these total reflected particles, the positive ions account for 15% with incident ion energies below 10 keV, for approximately 50% with 40 keV ions, and for nearly 80% with 100 keV ions.[2] The ratio of the flux of all emerging particles to the incident ion flux is nearly 0.9 for 100 eV hydrogen ions impinging on a metal surface.[2] Thus for a hydrogen plasma with a temperature of less than 1 keV, a maximum ratio of reflected ion flux to incident ion flux is would be less than 0.14. Since the dominant charge state of the emerging flux is neutral, extensive research has been conducted on the interaction of the reflected neutrals with the background plasma.[3,4] However, emphasis in the present study is on plasma sheath effects, so that only reflected ions and not reflected neutrals will be modeled here.

Ion reflection substantially increases the potential drop across the collector sheath which then increases the incident ion energy and so enhances the sputtering of collector surface material. The flux of these reflected ions increases the ion density at the source and so raises the total flux of ions striking the collector and the total energy transported from the plasma source to the surface. A strong two-stream interaction may occur between the primary ion and reflected ion streams which enhances potential fluctuations. With a small fraction of energy absorption by the

collector for each reflection event, the potential drop across the source sheath goes to zero.

This sheath region near the reflective surface is rich in kinetic behavior, having non-Maxwellian velocity distributions of the electrons and primary ions and reflected ions. Time-dependent computer simulations using particles are a prime tool for examining these non-neutral plasma regions and following the dynamics of the two-stream interaction. These simulations provide insight for verifying and improving the kinetic model for the steady state conditions. Consequently, both time-independent, kinetic theory and dynamic simulation to analyze this region.

The conceptual evolution from the fully bounded plasma to the present theoretical and simulation model of the sheath region is shown in Fig. 1. In many devices, a plasma source of Maxwellian ions and electrons may be distributed across a region several orders of magnitude larger than a plasma Debye length λ_D. This source may be generated over this distance by some mechanism (e.g. electron beam or photoionization). Emmert *et al.*[5] describe such a plasma source region which produces the first potential profile shown at the top of Fig. 1. The electrostatic potential falls to ϕ_P over the source region and then falls again to ϕ_C through the collector sheath. In the model of the present analysis, shown in the middle profile, the plasma source is the plane at $x=0$. Hence the potential drop through the distributed source region occurs fully within a few λ_D from the planar source; this "source sheath" is observed via simulation and described in the previous paper.[6] We find that ion reflection at the collector affects the source sheath as well as the collector sheath.

The planar plasma source emits steady and equal fluxes of ions and electrons, each with half-Maxwellian velocity distributions. The temperature and mass ratios of the ions and electrons are specified. These particles flow to a surface, which is

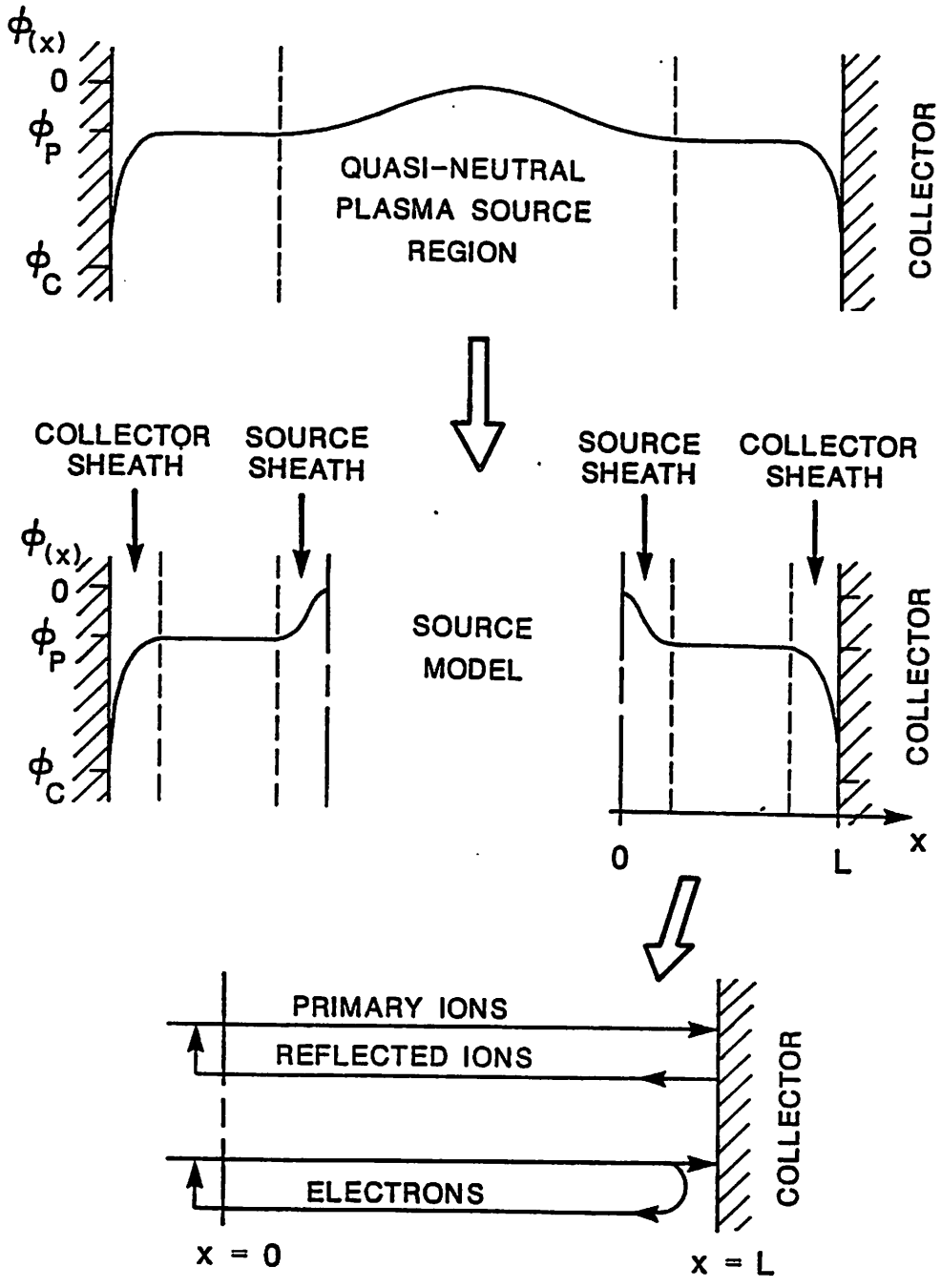

FIG. 1. Model and form of the electrostatic potential profile for the non-Maxwellian sheath region between a Maxwellian plasma source and an electrically floating collector that reflects primary ions. The top figure indicates the form of the potential profile for a distributed source. The source region is many orders of magnitude longer than the collector sheath region. The middle shows the potential profile expected for a planar source. The bottom diagrams the flow of particles between the source plane and collector.

electrically floating at potential ϕ_C and becomes charged by the incident particles. This collector plate returns and is discharged by a flux of reflected ions, F_r, which is a specified fraction of the incident primary ion flux F_i according to the ion reflection coefficient, $\zeta = -F_r/F_i$, where $\zeta > 0$.

The effect of a collector material, containing finite mass atoms, is modeled through the variation of $\alpha = -V_r/V_i$, the ratio of reflected velocity V_r to incident velocity V_i for each reflection event. For an elastic backscattering event, then $\alpha = (A-1)/(A+1)$ where A is the ratio of collector atom mass to incident ion mass.[7] For a hydrogen plasma and most collector materials, α is minimally 0.9; for an infinitely massive target, $\alpha = 1$. In my simulations, $\alpha = 0.9$ and $\alpha = 1$ are studied.

Particles returned to the source plane at $x = 0$ are added to the steady injected flux and are re-injected at the source temperature, as indicated in the bottom sketch of Fig. 1. These particles are mostly electrons which have been repelled by the source and collector sheath fields or are reflected ions which have been decelerated by the field yet have sufficient energy to reach $x = 0$. This "refluxing" at the source plane prevents any charge accumulation there and thus enforces a zero electric field at $x = 0$. Therefore the reflected ions reaching the source plane are assumed to interact in the plasma source region in such a way that they are heated to the ion source temperature. For the primary ions, the effective source density emitted into the region is increased beyond the source density injected because of refluxed, reflected ions (as will be demonstrated in Sec. II C 2). In addition, the source density of emitted electrons depends on ψ_C (a variable parameter) as caused by the refluxing of repelled electrons at $x = 0$, as demonstrated previously[6] in Sec. II C 2.

These boundary conditions model the source and collector sheath regions of a symmetric, bounded plasma with a central, full-Maxwellian source region. The region between the plasma source and collector is treated as collisionless; the plasma

region is implied collisional. These assumptions and boundary conditions, with the exception of the ion reflection at the collector, are identical to those given in a previous paper which analyzes the sheath region near a purely absorbing collector.[6]

The source and collector sheaths, sketched in the middle of Fig. 1, serve, respectively, to neutralize the injected source plasma and to maintain a zero net current at the floating collector. The potential drop across the source sheath, ϕ_P, becomes more negative as the ion/electron source temperature ratio, $\tau = T_{Si}/T_{Se}$, is decreased. (Throughout this paper, temperatures are measured in energy units.) The potential drop across the collector sheath, $\phi_C - \phi_P$, becomes more negative as the inverse mass ratio, $\mu = m/M$, is increased.

For a deuterium-tritium (D-T) plasma (with a mean value of $\mu = 1/4590$) and $\tau = 1$, varying the ion reflection coefficient ζ from 0 to 0.2 increases the density of ions in the system. Overall this increase creates a more negative potential curvature, $\nabla^2\phi$, which causes $e\phi_C$ to drop from $-3.32\,T_{Se}$ to $-3.72\,T_{Se}$. (The unsigned charge e is equal for all three species.) The potential drop across the source sheath, $e\phi_P = -0.34\,T_{Se}$, is unchanged by ζ at $\alpha = 1$. (For $\zeta = 0$, a detailed discussion of the source and collector sheath evolution including the derivation of the dependence of both ϕ_P and ϕ_C on μ and τ is provided elsewhere.[6])

If even a small fraction of impact energy is absorbed by the collector, the reflected ions have insufficient energy to return to the plasma source. The net result of setting $\alpha < 1$ is that the potential drop across the source sheath goes to zero. Thus the values of ϕ_C and ϕ_P depend on the value of α. A monotonically decreasing potential profile exists only for $1 \leq \alpha \leq \alpha_{min}$, where α_{min} depends on mass and temperature ratios. For a D-T plasma with $\tau = 1$ and $\zeta = 0.2$, then $\alpha_{min} = 0.993$, as obtained from the kinetic theory. The assumption of finite mass collector atoms ($\alpha < 1$) changes the potential profile but only slightly affects the overall potential

drop to the collector. For example, again for a D-T plasma with $\tau = 1$ and $\zeta = 0.2$ but with $\alpha = 0.993$, then $e\phi_C = -3.70\, T_{Se}$. This collector potential is slightly less than the result using $\alpha = 1$ as above.

Our bounded, electrostatic simulation utilizes the particle-in-cell method for one dimension in space x and velocity v. The time-evolution of the initially empty region is monitored until a steady-state configuration is achieved. The transient response and oscillations of the collective plasma behavior are measured. Because the simulation generates the velocity distribution of the ions and electrons in space and time, spatial profiles and time histories of various energy and particle fluxes are calculated.

The kinetic theory models the steady state configuration of the region and satisfies Poisson's equation and the Vlasov equation for each species applied to a potential profile which monotonically decreases from the source to the collector. The full kinetic description of both types of ions and of electrons determines the exact dependence of all three densities on the potential profile. With this description, various energy and particle fluxes are then derived as a function of potential at any spatial location.

The boundary conditions of zero electric field at the source and zero total current at the collector, with fixed coefficients of flux reflection ζ and velocity reflection α, are applied in the above kinetic analysis. The electric field is also assumed to be zero at the inflection point in potential, defined as ϕ_P, which occurs in the central region separating source and collector sheaths by many Debye lengths. Recall also that the magnitude of the velocity distribution, dependent on N_{Se}, of the emitted primary electrons is not fixed but dependent on ϕ_C because the electrons with $v < 0$ at $x = 0$ are refluxed. Using Poisson's equation and the above assumptions and conditions, the values of potential at the neutral region, ϕ_P (also defined as the source

sheath drop), and at the collector, ϕ_C, are calculated as a function of inverse mass and temperature ratios, μ and τ, and flux and velocity reflection coefficients, ζ and α.

The effect of ion reflection on the collector sheath region of a plasma source with $T_{Si}/T_{Se} \ll 1$ is also considered. Differing from those above, the boundary conditions are now assumed to be charge neutrality and a zero electric field at the plasma source at infinity. A Bohm condition[8] on minimum ion energy entering the collector sheath region is derived. (This minimum energy usually results from the acceleration caused by a source sheath.) A Boltzmann factor describes the potential dependence of electron density. A simple expression is derived for the dependence of potential drop across the collector sheath on mass ratio and ion reflection coefficient. Surprizingly, this expression agrees well with the more complete kinetic results for ψ_C but only for the case of $T_{Si}=T_{Se}$.

Details of both analyses are provided later in Sec. II. The numerical simulation model and results are presented and compared to kinetic analysis in Sec. III. In Sec. IV is detailed description of how this kinetic model differs from a previous study. Conclusions are given in Sec. V.

B. Historical review

Unlike other thoroughly studied collector effects, such as secondary electron emission or sputtering of surface material, the effect of the reflection of plasma ions on the sheath region has been investigated primarily by Brooks.[9] Data become available only within the last ten years on the charged fraction of backscattered particles caused by medium energy, light ions striking a surface.[1] As mentioned in Sec. I A, the predominant reflection event generates backscattered neutrals. The collisional interaction of these neutrals with the plasma far beyond the collector sheath has also been extensively analyzed and is beyond the scope of this paper.

Brooks[9] numerically solves time-independent Vlasov-Poisson equations in the collector sheath region. He combines the effect of secondary electron emission with ion reflection in the prediction of potential drop across the collector sheath and energy transported to the collector surface. An exact expression for these is not derived so that our results can only be compared for the set of parameters which Brooks has analyzed. In particular, he varies the coefficients of ion reflection and secondary electron emission at the boundary for a D-T plasma with $T_{Si}=0.25\,T_{Se}$.

II. THEORY

A. Model and assumptions

The source and collector sheaths charaterizing a bounded, symmetric plasma, as shown in the middle sketch of Fig. 1, is modeled over the region $0 < x < L$. A plasma source at the reference potential, at $x=0$, emits temporally constant, equal fluxes of ions and electrons, each with a half-Maxwellian distribution of velocity. The ratio of electron to ion mass, $\mu=m/M$, is a fixed parameter as well as the ratio of ion to electron source temperature, $\tau = T_{Si}/T_{Se}$. At $x=0$, the electric field is zero because of refluxing which permits no surface charge to accumulate there.

At $x = L$, the collector electrically floats to ϕ_C, is charged by all incident particles and is discharged by the reflected ions. The collector reflects incident ions with a velocity of $-\alpha\, V_i$ where V_i is incident ion velocity. The reflected flux F_r equals $-\zeta F_i$ which for this steady state analysis is temporally constant. The velocity and flux reflection coefficients, α and ζ, are fixed parameters. Net electrical current at the collector is zero as the collector is electrically isolated from the external world.

The value of potential at the neutral or inflection point, where $\nabla^2\phi=0$, between the source and collector sheaths is designated ϕ_P. The electric field $-\nabla\phi$ at ϕ_P,

which by definition is a constant, is chosen to be zero when the source and collector sheaths are many Debye lengths apart.

B. Derivation of velocity distributions

The velocity distribution functions for the time-independent model are governed by conservation of energy, as described in Sec. II A of the previous paper.[6] The electrostatic potential is assumed to be monotonically decreasing with position. Consequently, the velocity distribution of the primary ions is an accelerated half-Maxwellian; all ions reach the collector. The source and collector potential drops repel most of the electrons; only the fastest electrons reach the collector. Hence, the electron velocity distribution is a truncated, decelerated Maxwellian.

The reflected ions are decelerated as they leave the collector. Their velocity depends on that of the incident ions which cause a reflection event at the collector. All reflected ions are assumed to reach the source at $x = 0$. (In the simulations with $\alpha = 0.9$, some reflected ions will return to the collector.) As a result, using conservation of energy for primary and reflected ions and the definition of α, the minimum (slowest reflected ion) velocity, $-V_{Mr}$, can be expressed as

$$-V_{Mr}(x) = \left[\frac{2}{M}(e\phi_C - \alpha^2 e\phi_C - e\phi(x))\right]^{1/2}. \tag{1}$$

Thus the velocity distribution of the reflected ions, f_r, depends on potential as

$$f_r(\psi, v) = N_{Si}\left(\frac{M}{2\pi\tau T_{Se}}\right)^{1/2} \exp\left(\frac{\psi_C - \alpha^2\psi_C - \psi}{\tau\alpha^2} - \frac{\beta_r v^2}{\alpha^2}\right)\Theta(V_{Mr}(\psi) - v) \tag{2}$$

where v is particle velocity; N_{Si} is the primary ion density of the full-Maxwellian source (at $x = 0$); ψ is normalized potential $e\phi/T_{Se}$; β_r is $M/(2\tau T_{Se})$; and Θ is the Heaviside step function. The derivations for ion and primary electron values of minimum velocity and velocity distributions, are presented in the previous

paper[6] and are valid here. Hence for any value of potential, the time-independent distribution function for each species (reflected and primary ions and electrons) in the collisionless sheath region is known.

C. Derivation of moments

1. *Definitions*

Determining the various moments for each species of particles using the distribution functions in Eq. (2) above and in Eqs. (1) and (2) of the previous paper[6] provides the potential dependence of each moment. The general definitions, which use the velocity moments to evaluate density N, particle flux F, drift velocity $\langle V \rangle$, temperature T, kinetic energy flux Q, and heat flux H, are presented in Sec. II C 1, from the previous paper. The examples shown are for the ions but the same expressions within each integral apply for reflected ions and electrons. For the reflected ions, the lower limit of integration is $v = -\infty$ and the upper is $V_{Mr}(\psi)$ (also negative). Terms for reflected ions, primary ions, and electrons will be denoted with subscripts r, i, and e, respectively.

2. *Reflected ion density and ion fluxes*

An evaluation of the first velocity moments for all three species shows that F_r, F_i, and F_e, are spatially constant. With no creation or annihilation of particles along $0 < x < L$ and when the loss rate of particles equals the injection rate then, $\partial N/\partial t = 0$ so that $\nabla \cdot \mathbf{F} = 0$, by conservation of particles. Thus in my one-dimensional system at steady state, $\mathbf{F}$ is spatially constant for each species.

The net particle fluxes emitted from the source are assumed to be temporally constant. The condition of zero collector current and the definition of ζ determines the flux balance at the collector. Both ion fluxes are normalized to the electron flux

$F_e(\psi)$, hereafter called F, and are expressed as

$$F_i = F/(1-\zeta) \tag{3}$$

and

$$F_r = -\zeta F/(1-\zeta). \tag{4}$$

Integrating $vf_r(v)$ over all velocities for the reflected ions gives the reflected flux as

$$F_r = -N_{Si}\alpha^2\left(\frac{\tau T_{Se}}{2\pi M}\right)^{1/2}. \tag{5}$$

The ion source density N_{Si} is proportional to F_i from Eq. (9) of the previous paper[6], hence, greater ion reflection increases N_{Si} according to $(1-\zeta)^{-1}$ from Eq. (3) above. Indirectly through ψ_C, greater ion reflection increases the electron source density N_{Se} according to $\exp(-\psi_C)$ from the previous Eq. (10). Consequently, the above Eq. (3) and previous Eqs. (9) and (10) provide the neutralization parameter (i.e. the ratio of ion/electron densities emitted by the source) as equal to

$$N_{Si}/N_{Se} = (\mu\tau)^{-1/2}(1-\zeta)^{-1}\exp(\psi_C).$$

Substituting Eqs. (4) and (5) into the integral of Eq. (2), expressed in terms of F, yields the reflected ion density:

$$N_r(\psi) = \frac{\zeta F}{\alpha(1-\zeta)}\left(\frac{\pi M}{2\tau T_{Se}}\right)^{1/2}\exp\left(\frac{\psi_C - \alpha^2\psi_C - \psi}{\tau\alpha^2}\right)$$
$$\times\ \mathrm{erfc}\left(\frac{\psi_C - \alpha^2\psi_C - \psi}{\tau\alpha^2}\right)^{1/2}. \tag{6}$$

The density expressions in Eqs. (11) and (12) for $N_i(\psi)$ and $N_e(\psi)$ of the previous paper[6] are the same here if the F factor in Eq. (12) for the primary ions is replaced with $F/(1-\zeta)$.

3. *Reflected ion temperature and energy fluxes*

With the collisionless sheath model, temperature is defined as the mean square deviation of the velocity about the mean. With this definition, the dependence of reflected ion temperature on potential becomes

$$\frac{T_r(\psi)}{\tau T_{Se}} = \frac{1-(2/\pi)^{1/2}M^{3/2}(\alpha^2\tau T_{Se})^{-3/2}G(\beta_r, V_{Mr}(\psi))}{\operatorname{erfc}\left[\tau^{-1}\alpha^{-2}(\psi_C-\alpha^2\psi_C-\psi)\right]^{1/2}} - \frac{2\exp\left[-2\tau^{-1}\alpha^{-2}(\psi_C-\alpha^2\psi_C-\psi)\right]}{\pi\left\{\operatorname{erfc}\left[\tau^{-1}\alpha^{-2}(\psi_C-\alpha^2\psi_C-\psi)\right]^{1/2}\right\}^2} \tag{7}$$

where

$$G(\beta, y) = \int_0^y v^2 \exp\left(-\beta v^2\right) dv.$$

This normalized temperature is independent of source temperature T_{Se}. Note that the reflected ion temperature at the source plane is $T_r(0) = \tau T_{Se}(1-2/\pi)$, for ion reflection from infinite mass collector atoms ($\alpha = 1$).

The temperature expression in Eq. (7) is written so that the first term equals $M\langle V_r^2\rangle/\tau T_{Se}$ and the second term equals $M\langle V_r\rangle^2/\tau T_{Se}$. Primary and reflected ion temperatures are sensitive indicators of time-dependent beam heating not accounted for by this analysis using energy conservation. This analytic evaluation of $T_r(\psi)$ and results from simulation will be compared in Sec. IV.

Next, kinetic energy flux Q is determined in evaluating the third velocity moment. Often, Q is normalized with FT_{Se} and referred to as the energy transmission factor or power transmission coefficient δ. Integrating $v^3 f_r(\psi, v)$ over all velocities and dividing by FT_{Se} determines δ_r as

$$\delta_r(\psi) = -\zeta(1-\zeta)^{-1}(\alpha^2\tau - \alpha^2\psi_C + \psi_C - \psi).$$

(The reflected ion energy transmission factor δ_r is negative because energy is carried to the left, away from the collector.) Also including the full-Maxwellian distributions

in the two transverse directions then gives

$$\delta_r(\psi) = -\zeta(1-\zeta)^{-1}(2\alpha^2\tau - \alpha^2\psi_C + \psi_C - \psi).$$

From derivations in the previous work and, again, contributions from the transverse directions in velocity, then δ for the primary ions can be expressed as

$$\delta_i(\psi) = (1-\zeta)^{-1}(2\tau - \psi), \tag{8}$$

and for the electrons as

$$\delta_e(\psi) = 2 + \psi - \psi_C. \tag{9}$$

Combining these three equations gives the total energy transmission factor δ_T as

$$\delta_T(\psi) = \frac{-\zeta}{1-\zeta}(2\alpha^2\tau - \alpha^2\psi_C + \psi_C) + \frac{2\tau}{1-\zeta} + 2 - \psi_C \tag{10}$$

which is independent of position. When $\alpha = 1$ (infinite mass collector atoms) or when $\zeta = 0$ (purely absorbing collector), Eq. (10) provides identical expressions. With the mean kinetic energy defined as Q_α/F_α, Eqs. (8) and (9) show that ions arrive at the collector with a mean kinetic energy of $T_{Se}(2\tau - \psi_C)$ and electrons arrive with a mean kinetic energy of $2T_{Se}$.

A contribution to the kinetic or total energy flux is the heat flux, which indicates the thermal flow of thermal energy. The heat flux H is evaluated exactly in terms of the previously derived profiles using the definition given in Eq. (8) of the earlier paper. The form of H_r for reflected ions is the same as that for the other species except with F replaced by $-\zeta F/(1-\zeta)$; hence,

$$H_r(\psi) = Q_r(\psi) + \frac{3\zeta}{2(1-\zeta)}FT_r(\psi) + \frac{\zeta}{2(1-\zeta)}FM\langle V_r(\psi)\rangle^2.$$

D. Derivation of $\psi_C(\mu,\tau,\zeta,\alpha)$ and $\psi_P(\mu,\tau,\zeta,\alpha)$

With reference to Fig. 1, the potential is characterized by $\nabla^2\psi_P = 0$ somewhere between the source and collector sheaths. Hence, setting the net charge density to zero in Poisson's equation at this inflection point ψ_P gives $N_e(\psi_P) = N_i(\psi_P) + N_r(\psi_P)$. Substituting $N_i(\psi_P)$ and $N_e(\psi_P)$ (with F adjusted), from Eqs. (11) and (12) of the earlier paper,[6] into Poisson's equation provides the relation between ψ_C and ψ_P as

$$\exp(\psi_P-\psi_C)\Big[1+\mathrm{erf}(\psi_P-\psi_C)^{1/2}\Big] = \frac{1}{(1-\zeta)\sqrt{\mu\tau}}\exp\left(\frac{-\psi_P}{\tau}\right)\mathrm{erfc}\left(\frac{-\psi_P}{\tau}\right)^{1/2}$$
$$+\frac{\zeta}{\alpha(1-\zeta)\sqrt{\mu\tau}}\exp\left(\frac{\psi_C-\alpha^2\psi_C-\psi_P}{\tau\alpha^2}\right)\mathrm{erfc}\left(\frac{\psi_C-\alpha^2\psi_C-\psi_P}{\tau\alpha^2}\right)^{1/2}. \qquad (11)$$

Recall that the assumption of zero net electric current (floating collector) has been included in the solution for these densities.

A second equation relating ψ_C and ψ_P results from imposing the zero electric field condition at the inflection point ψ_P. Integrating Poisson's equation, $\nabla^2\psi = 4\pi e^2 T_{Se}^{-1}(N_e - N_i - N_r)$, once from $\psi = 0$ to $\psi = \psi_P$ and utilizing the zero field condition at these two points is equivalent to integrating Eq. (11) over the same limits. The resulting expression can be written as the sum of separate terms for the normalized integral densities $\mathcal{Z}$ for electrons and primary and reflected ions which respectively are

$$\mathcal{Z}_e = \exp(\psi_P-\psi_C)\Big[1+\mathrm{erf}(\psi_P-\psi_C)^{1/2}\Big] + \frac{2}{\sqrt{\pi}}(-\psi_C)^{1/2}$$
$$-\frac{2}{\sqrt{\pi}}(\psi_P-\psi_C)^{1/2} - \exp(-\psi_C)\Big[1+\mathrm{erf}(-\psi_C)^{1/2}\Big],$$
$$\mathcal{Z}_i = \frac{1}{1-\zeta}\sqrt{\frac{\tau}{\mu}}\left[\exp\left(\frac{-\psi_P}{\tau}\right)\mathrm{erfc}\left(\frac{-\psi_P}{\tau}\right)^{1/2} - 1 + \left(\frac{-4\psi_P}{\pi\tau}\right)^{1/2}\right],$$

and

$$\mathcal{Z}_r = \frac{\alpha\zeta}{1-\zeta}\sqrt{\frac{\tau}{\mu}}\left[\exp\left(\frac{\psi_C - \alpha^2\psi_C - \psi_P}{\tau\alpha^2}\right)\operatorname{erfc}\left(\frac{\psi_C - \alpha^2\psi_C - \psi_P}{\tau\alpha^2}\right)^{1/2}\right.$$
$$\left. -1 + \frac{2}{\sqrt{\pi}}\left(\frac{\psi_C - \alpha^2\psi_C - \psi_P}{\tau\alpha^2}\right)^{1/2}\right].$$

Thus the zero field condition at ψ_P is that the normalized integral densities sum to zero,

$$\mathcal{Z}_e + \mathcal{Z}_i + \mathcal{Z}_r = 0. \tag{12}$$

Together Eqs. (11) and (12) define the source sheath drop ψ_P and collector potential ψ_C in terms of the ratios of electron/ion mass μ, ion/electron temperature τ, and ion reflection coefficients for flux and velocity, ζ and α.

E. Evaluation of collector potential drop for $\tau \ll 1$

With the approach described in Sec. II D, the terms of Eqs. (11) and (12) cannot be evaluated for $\tau = 0$, because then the ion densities are infinitely large at $x = 0$. (This limit is discussed in detail in Sec. III E of the previous paper.[6]) Therefore, a different (more traditional) approach is described below. The acceleration provided by the source sheath is replaced by determining some minimum ion energy required to enter to the collector sheath which assures that the potential profile is monotonically decreasing (a Bohm condition[8]).

Consider a collector surface with floating potential ϕ_F (relative to potential just beyond the collector sheath), at spatial position $x = 0$, and in contact with a plasma at $x > 0$. (This model differs from that shown in Fig. 1.) Poisson's equation describes the normalized electrostatic potential with

$$\nabla^2\phi(x) = 4\pi e\left(n_e(x) - n_i(x) - n_r(x)\right) \tag{13}$$

where n_e, n_i, and n_r are the densities of electrons, primary ions and reflected ions. The reference potential far from the collector is $\phi(\infty)=0$. Charge neutrality occurs as $x\rightarrow\infty$, thus with $n_e(\infty)=n_\infty$ then

$$n_\infty = n_i(\infty) + n_r(\infty). \tag{14}$$

The densities which are substituted into Poisson's equation are derived for warm electrons and cold primary and reflected ions. Electrons are assumed to have a Maxwellian velocity distribution with temperature T. Thus their density, expressed with a Boltzmann factor, is

$$n_e(x) = n_\infty \exp\left(e\phi(x)/T\right). \tag{15}$$

With a temperature much less than T, primary ions arrive at the sheath edge with kinetic energy $\mathcal{E}$ (to be found later). All of these ions entering the sheath region reach the collector at $x=0$. Hence, with a temporally constant flux of incoming primary ions, F_i, continuity of particles and conservation of energy determines their density at any position x as

$$n_i(x) = n_i(\infty)\mathcal{E}^{1/2}\left(\mathcal{E} - e\phi(x)\right)^{-1/2}. \tag{16}$$

At the collector, all reflected ions leave with velocity v_{0r} equal to the incident primary ion velocity v_{0i} (for infinitely massive atoms in the collector). All reflected ions are assumed to reach the plasma source at infinity so that the reflected ion flux F_r is also spatially constant. By utilizing the condition of zero net collector current and the definition of ζ (as before), the reflected ion density becomes

$$n_r(x) = -F\zeta(1-\zeta)^{-1}v_r(x)^{-1} \tag{17}$$

where F is the net electron flux at the collector. Since collector atoms are assumed to have infinite mass, the reflected ions must also have total energy $\mathcal{E}$, independent

of x. With this energy conservation, the expression for reflected ion density from Eq. (17) yields

$$n_r(x) = -F\zeta(1-\zeta)^{-1}\left[\frac{2}{M}(\mathcal{E} - e\phi(x))\right]^{-1/2}. \tag{18}$$

The average velocity $\langle v_e \rangle$ of the half-Maxwellian velocity distribution of electrons reaching the collector is $(2T)^{1/2}(\pi m)^{-1/2}$. Because the electron density reaching the collector is half that of the full-Maxwellian distribution (Eq. (15)), then the electron flux, $F = n_e\langle v_e \rangle$, is expressed in terms of the collector sheath drop ϕ_F as

$$F = n_\infty T^{1/2}(2\pi m)^{-1/2}\exp(e\phi_F/T). \tag{19}$$

Substitution of this expression into Eq. (18) determines the final form of the reflected ion density as

$$n_r(x) = n_\infty\left(\mathcal{E} - e\phi(x)\right)^{-1/2}\frac{\zeta}{1-\zeta}\left(\frac{TM}{4\pi m}\right)^{1/2}\exp\left(\frac{e\phi_F}{T}\right). \tag{20}$$

Expressed in terms of $n_i(\infty)$ in Eq. (16), the primary ion density must be found also in terms of n_∞. The charge neutrality condition in Eq. (14) and the value for $n_r(\infty)$ in Eq. (19) for $\phi(\infty) \to 0$ yields the final form for the primary ion density as

$$n_i(x) = n_\infty\left(\mathcal{E} - e\phi(x)\right)^{-1/2}\left[\mathcal{E}^{1/2} - \frac{\zeta}{1-\zeta}\left(\frac{TM}{4\pi m}\right)^{1/2}\exp\left(\frac{e\phi_F}{T}\right)\right]. \tag{21}$$

The minimum value of $\mathcal{E}$, the ion energy at the collector sheath edge, is specified with the assumption of zero electric field, i.e. charge neutrality, at the plasma source. (Note that charge neutrality only assures a constant electric field; the zero field condition is an added requirement.) With the three densities, in Eqs. (15), (16), and (20), Poisson's equation in Eq. (13) takes the form of

$$(4\pi e n_\infty)^{-1}\nabla^2\phi(x) = \exp\left(e\phi(x)/T\right) - \mathcal{E}^{1/2}\left(\mathcal{E} - e\phi(x)\right)^{-1/2}. \tag{22}$$

As $x \to \infty$ approaching the plasma source, then $\phi(\infty) \to 0$ and $-\nabla\phi(\infty) \to 0$ with this zero field condition. The behavior of Poisson's equation for $x \to 0$ is investigated next. Multiplying Eq. (22) by $\nabla\phi$ and then integrating from ∞ to x yields

$$\frac{1}{4\pi T n_\infty}(\nabla\phi)^2 = \exp\left(\frac{e\phi(x)}{T}\right) - 1 + \frac{2\mathcal{E}}{T}\left[\left(1 - \frac{e\phi(x)}{\mathcal{E}}\right)^{1/2} - 1\right]. \tag{23}$$

Expanding $e\phi/T$ and $e\phi/\mathcal{E}$ in a Taylor series and retaining the first three terms determines that

$$\frac{1}{4\pi T n_\infty}(\nabla\phi)^2 \approx \frac{1}{2}\left(\frac{e\phi}{T}\right)^2 - \frac{(e\phi)^2}{4T\mathcal{E}}. \tag{24}$$

As $x \to \infty$ then the electric field, $-\nabla\phi$, is required to be always positive, while approaching zero and to ensure a real (non-oscillating) solution to potential; hence, $(\nabla\phi)^2 \geq 0$. When applied to Eq. (24), this limit implies that as $x \to \infty$

$$\mathcal{E} \geq T/2. \tag{25}$$

This is also the Bohm condition[8] for the minimum ion energy entering the sheath region near a purely absorbing collector.

This limit of minimum ion energy determines the exact dependence of potential on ζ. With the zero net collector current, then $F = (1 - \zeta)F_i$. Substituting this expression in Eq. (18) for electron flux provides

$$(1 - \zeta)F_i = n_\infty \exp\left(\frac{e\phi_F}{T}\right)\left(\frac{T}{2\pi m}\right)^{1/2}. \tag{26}$$

Leaving the plasma source, the ion current F_i equals $n_i(\infty)(2\mathcal{E}/M)^{1/2}$ by energy conservation. With this expression and $n_i(\infty)$ (for $\phi \to 0$) from Eq. (21), then Eq. (26) is re-arranged to obtain

$$\exp\left(\frac{-e\phi_F}{T}\right) = \frac{1+\zeta}{1-\zeta}\left(\frac{MT}{m4\pi E}\right)^{1/2}. \tag{27}$$

If the minimum ion energy is $T/2$, then

$$-\frac{e\phi_F}{T} = \ln\left[\left(\frac{1+\zeta}{1-\zeta}\right)\left(\frac{M}{2\pi m}\right)^{1/2}\right]. \tag{28}$$

F. Theoretical results

1. *Potential drops across the collector and source sheaths*

The full kinetic description in Sec. II D provides the two equations necessary to solve for ψ_C and ψ_P for a unique parameter set. The form of the dependence of ψ_C on ψ_P from Eqs. (11) and (12) is the same for most values of mass and temperature ratios and ion reflection coefficients for full reflected velocity ($\alpha = 1$). In Fig. 2 is shown the curves of neutrality (Eq. (11)) and zero field (Eq. (12)) for a D-T plasma with $\tau = 1$ and ion reflection of $\zeta = 0.2$. The simultaneous solution of these two curves occurs at two points. The common point where $d\psi_C/d\psi_P = 0$ on the zero field curve is the chosen value for ψ_C and ψ_P. The second common point occurs where $\psi_P = 0$, which is the trivial solution. (A detailed analysis of the behavior of these two curves is described in Sec. II D of the previous paper.[6])

As less energy is transferred to the reflected ion during a reflection event, i.e. α drops below 1, the common (non-trivial) solution of the two curves in Fig. 2 moves toward $\psi_P = 0$ for slightly smaller values of $-\psi_C$. Prior to reaching the common solution of $\psi_P = 0$, at some minimum value of α, the neutrality curve bends away from the zero field curve and only the trivial, common solution exists. For example, for $\mu = 1/40$ at $\tau = 1$ with $\zeta = 0.2$, this minimum value of $\alpha = 0.986$ generates the common solution of $(\psi_C, \psi_P) = (-1.38, -0.18)$; whereas with $\alpha = 1$ for the same plasma parameters, then $(\psi_C, \psi_P) = (-1.40, -0.30)$. These values will be compared in Sec. III with those generated via simulation. For a D-T plasma at $\tau = 1$ with $\zeta = 0.2$, the minimum value of $\alpha = 0.993$ generates the common solution of $(\psi_C, \psi_P) = (-3.70, -0.20)$; whereas with $\alpha = 1$, then $(\psi_C, \psi_P) = (-4.24, -0.86)$.

The curves in Fig. 3 indicate $\psi_C(\mu)$ and $\psi_P(\mu)$ for a range of $\zeta = 0$ (lower curves) to $\zeta = 0.2$ (upper curves) for three temperature ratios, $\tau = 0.1$, 1, and 10 for infinite mass atoms in the collector ($\alpha = 1$). Each curve comprises a family

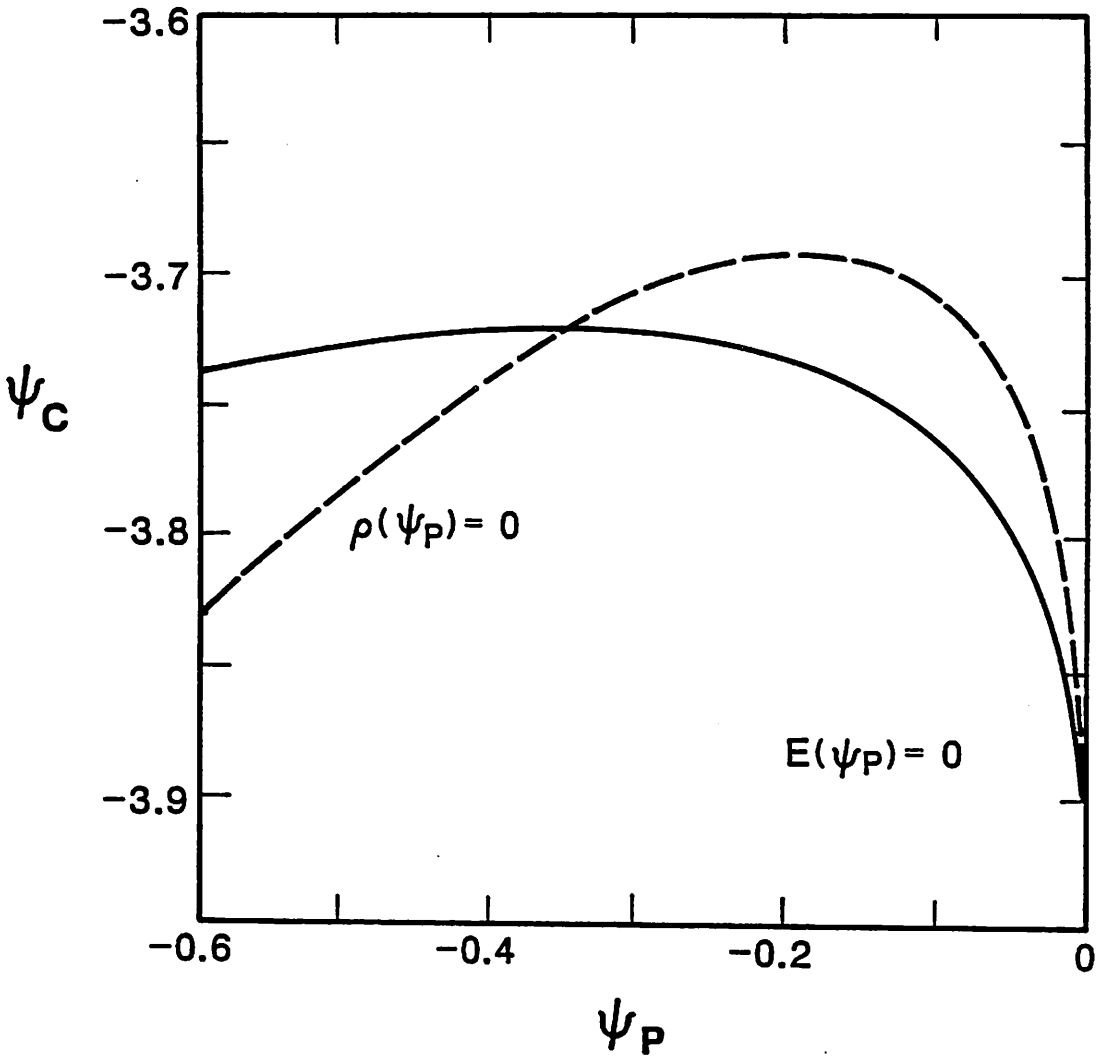

FIG. 2. Solutions of ψ_C vs. ψ_P with the neutral charge density ρ expression at ψ_P in Eq. (11) and the zero field E condition at $\psi=\psi_P$ and $\psi=0$ in Eq. (12) for a D-T plasma with $T_{Si}/T_{Se}=1$ at the source and an ion reflection coefficient of 0.2. The potentials are normalized as $\psi=e\phi/T_{Se}$.

of points determined from the common solution of Eqs. (11) and (12) at specific values of μ and τ; the generation of one such data point appears in Fig. 2. For a surface that absorbs a small fraction of the incident ion energy, these curves represent the maximum magnitudes of ψ_C and ψ_P for each ζ. For each set of μ and τ with $\alpha=1$, the presence of ion reflection does not affect ψ_P. (As discussed earlier with $\alpha=1$, then ion reflection causes $\psi_P \to 0$.) Over most of the range of μ and τ shown in Fig. 3, ion reflection raises the value of $-\psi_C$ consistently by 0.4 (for $\alpha=1$ and $\zeta=0.2$). The overall trends of the dependence of ψ_P and ψ_C on the mass and temperature ratios are discussed in the previous paper.[6]

The effect of ζ on ψ_C and ψ_P at a particular mass ratio for three temperature ratios is displayed in Fig. 4. Equations (11) and (12) are solved for ψ_C and ψ_P for $\mu=1/40$ and $1/4590$ with $\tau=0.1$, 1, and 10 for a wide range of reflection coefficients. The solid and dashed curves indicate $\psi_C(M/m,\tau)$ and $\psi_P(M/m,\tau)$, respectively. The low mass ratio of 40 is chosen to compare with simulation results in the next section; the large mass ratio of 4590 represents a D-T plasma. Increasing the ion reflection coefficient significantly increases the collector potential but, even over this exaggerated range, has little effect on the source sheath drop ψ_P (for $\alpha=1$).

The dot-dashed curve in Fig. 4 indicates the simple theory for the potential drop across the collector sheath ψ_F for cold ions, $\tau \ll 1$, from Eq. (28). An interesting coincidence is how this simple theory nearly matches the exact theory for warm ions, where $T_{Si}=T_{Se}$. These two theories agree for this wide range of both mass ratios and coefficients of ion reflection. Hence Eq. (28) provides a simple approximation for collector potential ψ_C (not potential drop across the collector sheath, $\psi_C-\psi_P$, which the simple analysis determines), only for equal source temperatures.

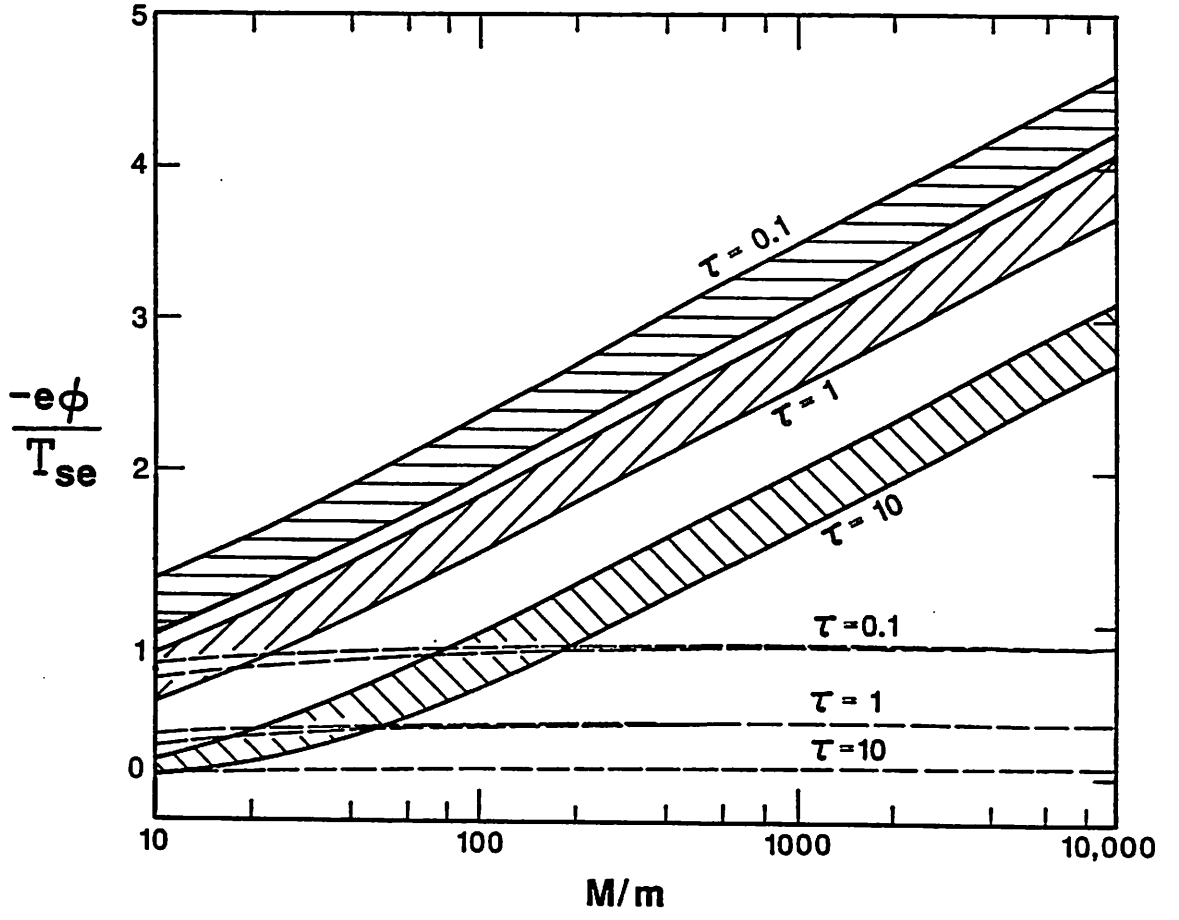

FIG. 3. Potentials at two locations for ion reflection coefficient of $\zeta = 0$ to $\zeta = 0.2$ for three source temperature ratios $\tau = T_{Si}/T_{Se}$ as a function of mass ratio, $1/\mu$. Collector potential ψ_C (solid curves) and source sheath potential drop ψ_P (dashed curves) are from kinetic theory. For each pair of curves (bounding the shaded region or in close proximity), the lower curve is the solution with $\zeta = 0$ and the upper curve is with $\zeta = 0.2$.

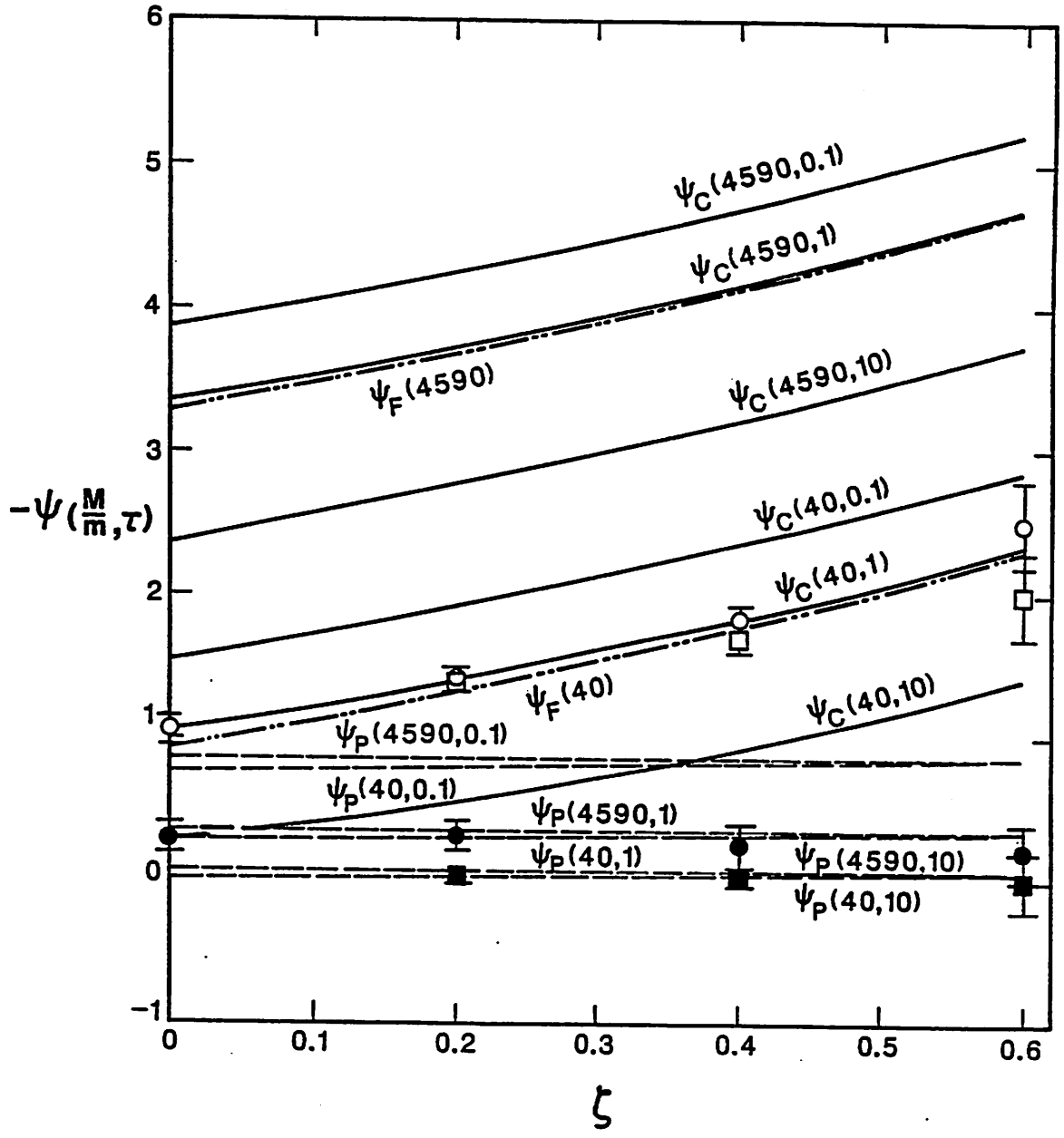

FIG. 4. Potentials at various locations for $M/m = 40$ and 4590 as a function of ion reflection coefficient ζ. Collector potential ψ_C (solid curves) and source sheath potential drop ψ_P (dashed curves) are from kinetic theory for three source temperature ratios $\tau = T_{Si}/T_{Se}$ with a velocity reflection coefficient of $-V_r/V_i = \alpha = 1$. Collector sheath potential drop ψ_F (dot-dashed curves) is from kinetic theory for cold ions $\tau \ll 1$ in Eq.(28). Data points indicate simulation values with $\alpha = 1$ for ψ_C (open circles) and ψ_P (closed circles) and with $\alpha = 0.9$ for ψ_C (open squares) and ψ_P (closed squares), all at $\tau = 1$; bars indicate oscillation amplitudes at each ψ_C and ψ_P. The potentials are normalized as $\psi = e\phi/T_{Se}$.

2. *Energy transport to the collector*

The effect of ion reflection on the total energy transport coefficient δ_T at the collector is displayed in Fig. 5. The value of $\psi_C(\mu, \tau, \zeta)$, which is calculated from Eqs. (11) and (12) and plotted in Fig. 3, determines $\delta_T(\psi_C)$ from Eq. (10) with $\alpha = 1$. The shaded areas indicate (for $\tau = 0.1$, 1, and 10) the range of $\delta_T(\zeta, \tau)$ generated by varying ζ from 0 to 0.2 at each mass ratio. Figure 5 shows the small increase in energy transported from the plasma to the collector as the ion reflection coefficient ζ is increased. The expressions for $\delta(\psi)$ for each species in Sec. II C 3 show that $\delta_e(\psi_C) = 2$ and $\delta_i(\psi_C) + \delta_e(\psi_C) = 2\tau - \psi_C$. Hence, energy transported by electrons is unaffected by ion reflection but the net energy transported by both ion species depends on ζ only indirectly via $\psi_C(\zeta)$.

The effect of ion reflection on the total energy transport coefficient at a particular mass ratio for three temperature ratios is displayed in Fig. 6. Equation (10) is solved for $\delta_T(\psi_C)$ for a wide range of reflection coefficients for $\mu = 1/40$ with $\tau = 0.1$, 1, and 10 and $\alpha = 1$. The collector potentials used in this equation are determined from Eqs. (11) and (12) and plotted in Fig. 4. (These values will be compared with simulation in the next section.) Energy transport coefficients δ_T are normalized to δ_T with no ion reflection, $\zeta = 0$, to show directly that increasing ζ increases the total energy transported to the collector. This dependence is strongest for cooler ions. When $\tau = 10$, increasing ζ has little effect on δ_T because the dominant contribution to δ_T then is from the large ion thermal energy.

Ion reflection slightly increases the mean kinetic energy of ions reaching the collector which will increase the sputtering rate of surface material back into the plasma, as demonstrated in Fig. 7. Mean kinetic energy W is defined as the kinetic energy flux Q_i divided by the particle flux F_i. Thus from Eq. (8), $W = T_{Se}(2\tau - \psi_C)$. Values are normalized to W at $\zeta = 0$ and plotted for $\mu = 1/40$ with $\tau = 0.1$, 1, and

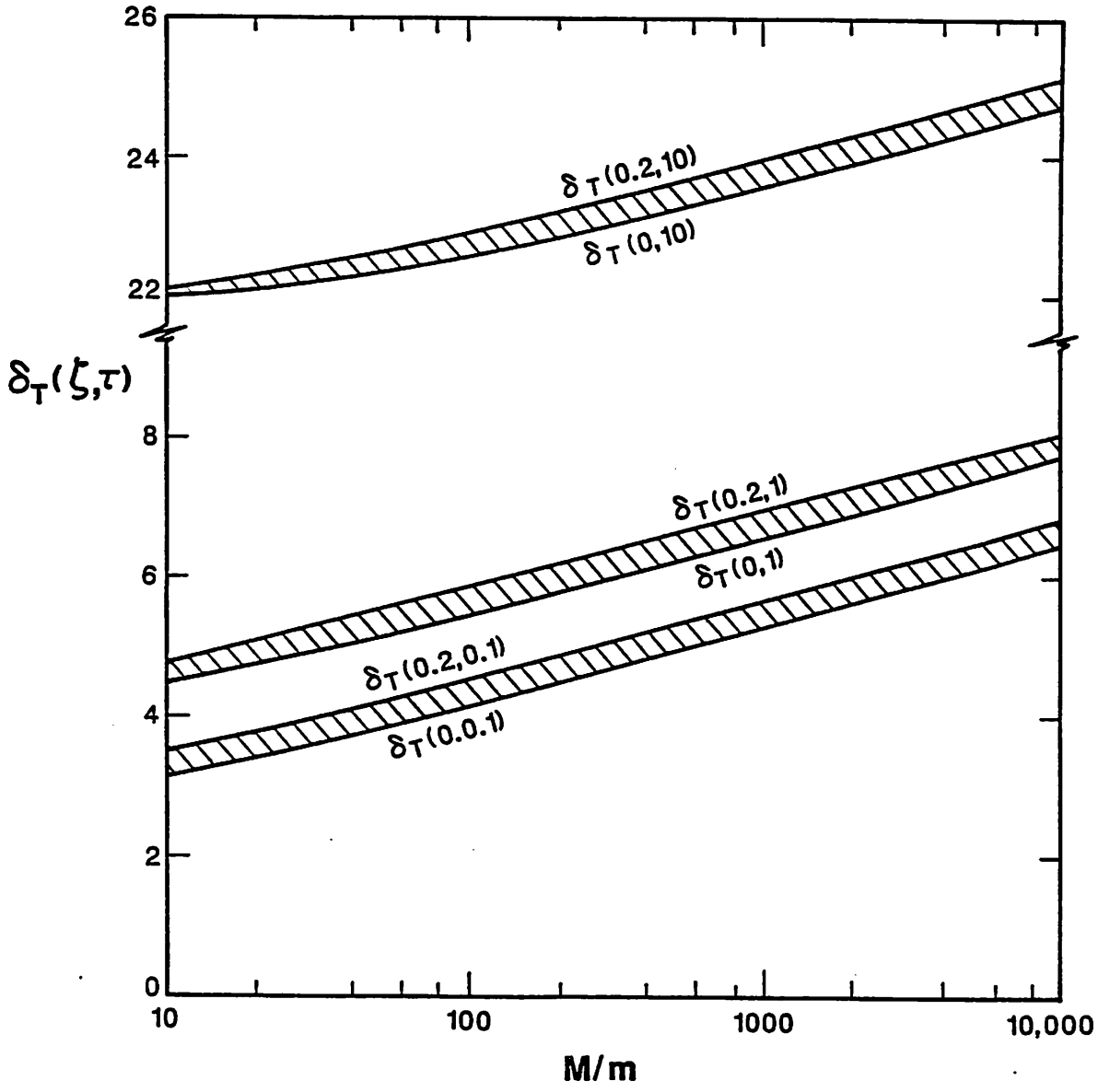

FIG. 5. Total energy transport coefficient δ_T at ion reflection coefficients of $\zeta = 0$ and $\zeta = 0.2$ for three source temperature ratios $\tau = T_{Si}/T_{Se}$ as a function of mass ratio, $1/\mu$ with complete velocity reflection, $\alpha = 1$. The region containing the solution of δ_T, with ζ varied from 0 to 0.2, is shaded for each τ. Analysis assumes Maxwellian velocities in the two directions transverse to x.

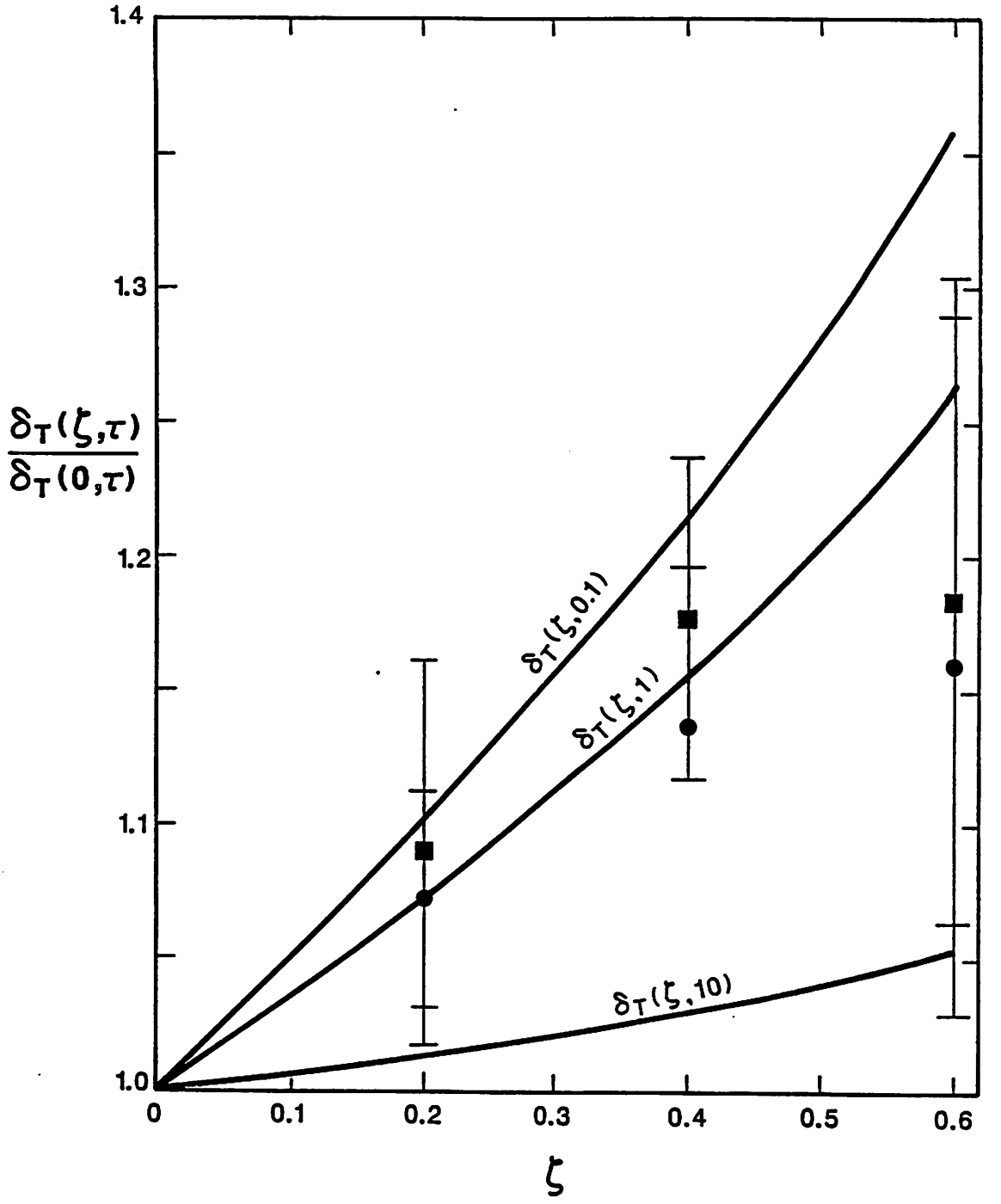

FIG. 6. Total energy transport coefficient δ_T as a function of the ion reflection coefficient ζ at $M/m=40$ with three source temperature ratios $\tau=T_{Si}/T_{Se}$. Solid curves indicate the kinetic theory results with $-V_r/V_i=\alpha=1$. Data points indicate simulation values with $\alpha=1$ (circles) and with $\alpha=0.9$ (squares), each at $\tau=1$; bars indicate oscillation amplitudes of δ_T. Values of δ_T are normalized to δ_T at $\zeta=0$. Analysis assumes Maxwellian velocities in the two directions transverse to x.

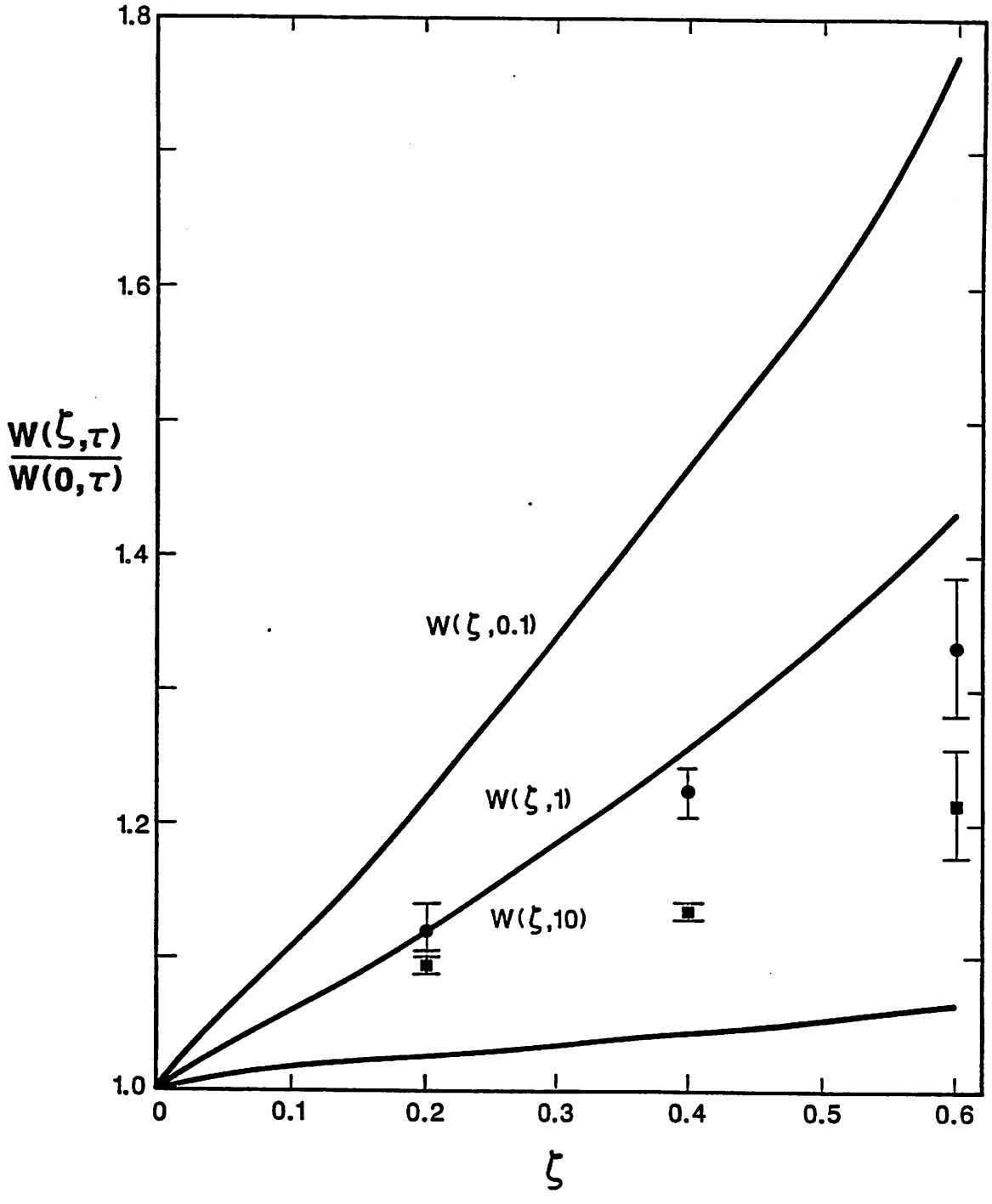

FIG. 7. Mean ion kinetic energy W at the collector as a function of the ion reflection coefficient ζ at $M/m=40$ with three source temperature ratios $\tau=T_{Si}/T_{Se}$. Solid curves indicate the kinetic theory results. Data points indicate simulation values with $\alpha=1$ (circles) and with $\alpha=0.9$ (squares), each at $\tau=1$; bars indicate oscillation amplitudes of W. Values of W are normalized to W at $\zeta=0$.

10. Note that these curves represent changes in mean ion energy and not the ion energy transport coefficient which differs by a factor of $(1-\zeta)^{-1}$.

Compared with a purely absorbing surface, a reflecting collector surface composed of infinite mass atoms creates an additional particle flux of ions, which increases $|\psi_C|$ to maintain the current balance. Because the reflected ion flux (with $v<0$) away from the collector remove the energy that the returning (refluxed) ion flux (with $v>0$) carries to the collector, the total energy transported to the collector only increases with $|\psi_C(\zeta)|$ and is not directly affected by ζ.

III. SIMULATION

A. Simulation description and fixed parameters

A particle-in-cell computer simulation for ions and electrons is used to study the plasma-sheath region bounded by a Maxwellian plasma source and an absorbing collector which reflects a fraction of incident primary ions. Lorentz forces move the particles via electric fields derived self-consistently on a fixed mesh with Poisson's equation solved for each time step. Particles are linearly weighted to each grid where the velocity distributions are evaluated. (Methods used are described in Birdsall and Langdon's book.[10] The code used here is fundamentally PDW1 developed by Lawson,[11] with surface effects and transport evaluation added.)

The simulation region, $0 \leq x \leq L$ shown in Fig. 1, is initially empty. Particle electrons and ions with a mass ratio M/m of 40 are injected with equal and temporally constant fluxes. Both species enter the region at $x=0$ with a half-Maxwellian velocity distribution with a primary ion/electron temperature ratio of $\tau=1$. Maximum velocity values injected at the source or collector are 6 times the thermal velocity. As shown in the bottom sketch in Fig. 1, the particles that return to the source at $x=0$ are re-inserted as injected particles with a velocity characteristic

of the source temperature. No charge accumulation is allowed at the source plane; hence, the electric field at $x=0$ remains zero. At $x=L$, incident and reflected particles charge and discharge the electrically floating collector.

Reflected ions which originate at $x=L$ have a velocity distribution dependent on the incident ion velocity distribution. The reflected velocity ratio, $\alpha=-V_r/V_i$ is chosen to be 1 or 0.9. For $\alpha=1$, the algorithm used to determine the reflected ion velocity must conserve energy as accurately as the particle mover algorithm. The derivation of the reflection algorithm used is presented in the appendix. The parameter value $\alpha=0.9$ represents energy lost to collector atoms during a reflection event, as defined in Sec. I A. The incident ions which cause a reflection are chosen such that the time-averaged ratio of reflected ion flux F_r to incident primary ion flux F_i equals the fixed parameter $-\zeta$.

B. Variable parameters

Time histories and spatial profiles are presented for electrostatic potential and field, velocity scatter, temperature, and energy transport. Results are concentrated primarily on the ion reflection effects. Because generally the potential profile decreases monotonically, as before with no reflection, the theory for and profiles of density, drift velocity, temperature, kinetic energy flux, and heat flux for ions and primary electrons (which are presented in Figs. 5(a)–5(h) in the previous paper[6]), have the same potential dependence as do the profiles when ion reflection is included.

Except for potential and velocity scatter plots, all profiles are time-averaged over one plasma period from the last simulation time step after steady state is attained. Potential and scatter plots are not time-averaged but are snapshots at the last time step. Steady state occurs when the average number of particles in the system becomes approximately constant with time. Time steps are typically $0.05/\omega_P$, where ω_P is the spatially averaged plasma frequency.

Systems studied are 27–46 Debye lengths (λ_D) long and are resolved with from 3–5 grid cells per λ_D. This plasma Debye length is based on the steady state, length-averaged value of electron density $\overline{N}_e$ which increases with $-\psi_C$ for a constant injected flux. A density of at least 400 particle electrons in $1\lambda_D$ is required for reduction of noise to a level below $\pm 10\%$.

C. Results for $M/m=40$ and $\tau=1$

1. *Time-dependent behavior*

a. Electrostatic potential. The temporal behavior of the collector potential ψ_C and source sheath drop ψ_P for $\zeta=0.2$ with $\mu=1/40$ and $\tau=1$ is displayed with the history plots shown in Fig. 8. (These plots show only the first half of the potential histories.) The potentials measured at $x/L=0.5$ and 1 are those plotted respectively as ψ_P and ψ_C.

The effect of varying the energy absorbed by the collector is seen in comparing Fig. 8(a) for $\alpha = 1$ with Fig. 8(b) for $\alpha = 0.9$. Potentials are normalized with e/T_{Se}. Typically ψ_C and ψ_P fluctuate with frequency ω_P which depends on $\overline{N}_e$. For reference, the calculated value of twenty plasma periods is indicated next to the potential curves by the double arrow. The unit of time t in these and subsequent plots is L/V_{te} where where the electron thermal velocity, $V_{te} = (T_{Se}/m)^{1/2}$. The amplitude of the oscillations in ψ depends on the number of simulation particles N_D in a Debye length. For $N_D \approx 400$, the amplitude is $\pm 10\%$ of ψ.

In Figs. 8(a) and 8(b), the early transient responses of ψ_C and ψ_P for both simulations are identical. The collector potential begins at zero and then dips to 3.2 times the final, averaged value of $\psi_C = -1.4$. The most negative value of ψ_C occurs when the faster electrons (with a velocity of 1.7 V_{te}) reach the collector. At this time, ions experience their strongest acceleration toward $x=L$. The source sheath

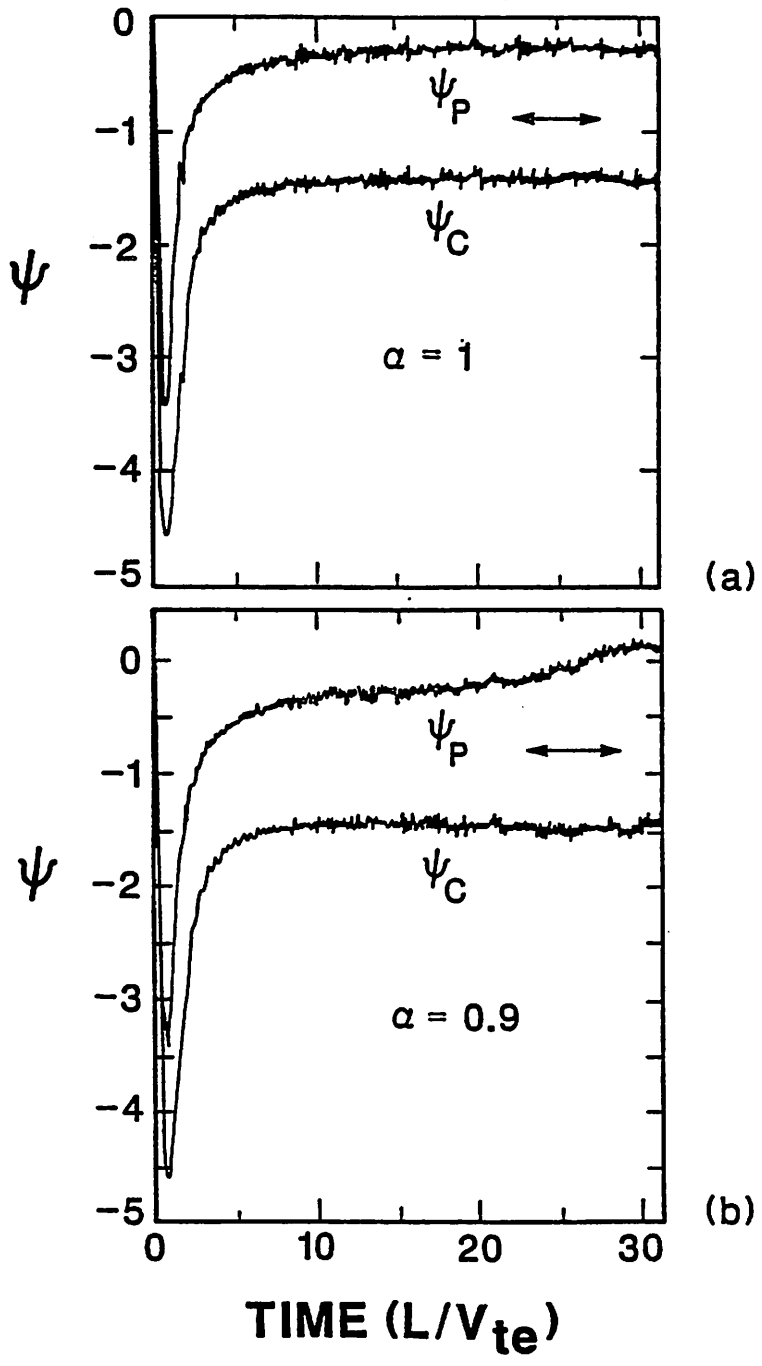

FIG. 8. Early time histories of collector potential and source sheath potential drop from simulation with (a) $-V_r/V_i = \alpha = 1$ and (b) $\alpha = 0.9$ for an ion reflection coefficient of $\zeta = 0.2$, $M/m = 40$, and $T_{Si}/T_{Se} = 1$. The system lengths L are (a) $27\,\lambda_D$ and (b) $30\,\lambda_D$. Arrows indicate the calculated value of 20 plasma periods determined from the length-averaged electron density. The potentials are normalized as $\psi = e\phi/T_{Se}$ and are measured respectively at $x = L$ and $0.5L$.

potential drop also begins at zero and then dips to 11 times the averaged value of $\psi_P = -0.3$.

A difference between the two simulations occurs at times beyond $15\,L/V_{te}$. For $\alpha = 1$ in Fig. 8(a), the $\psi_P = -0.3$ is the final value; however, for $\alpha = 0.9$ in Fig. 8(b), for time beyond $15\,L/V_{te}$, ψ_P begins to approach zero and eventually becomes positive. (When $\psi_P > 0$, the potential profile does not decrease monotonically away from the source plane which is contrary to theoretical assumptions.) At a later time (not shown), ψ_P returns to and equilibrates at $\psi_P = -0.02$. The interaction of the primary ion and reflected ion streams (shown next) uses this change in potential profile with time.

b. Ion velocity space. The transition from early to final stages of the simulation with $\alpha = 1$ is shown in the snapshots of velocity scatter plots of primary and reflected ions in Figs. 9(a)–9(d) at times of 15.6, 23.4, 31.2, and 62.5 (in units of L/V_{te}). In these scatter plots, primary ions, with positive velocities, are indicated by dots and reflected ions, mostly with negative velocities, are indicated with plusses.

As seen with the potential history in Fig. 8(a), although ψ_C has equilibrated by $t = 15.6$, it is still too early in the simulation for energy conservation to apply to all the ions in Fig. 9(a). At this time, the minimum reflected ion speed is not quite zero at $x = 0$. (If the system is static, then zero velocity ions are expected.) The transit time of slower reflected ions with an average velocity of an ion thermal velocity $V_{ti} = (\tau T_{Se}/M)^{1/2}$ is $L/V_{te}(\mu\tau)^{-1/2}$. For $\mu = 1/40$ and $\tau = 1$, this transit time is roughly $6\,L/V_{te}$. The reflected ions near the source plane in Fig. 9(a) have experienced an earlier slightly more negative potential profile from their creation at the collector when $t = 9$. In addition, the primary ions which caused their reflection have been created when $t = 3$ and have experienced an even greater negative potential profile.

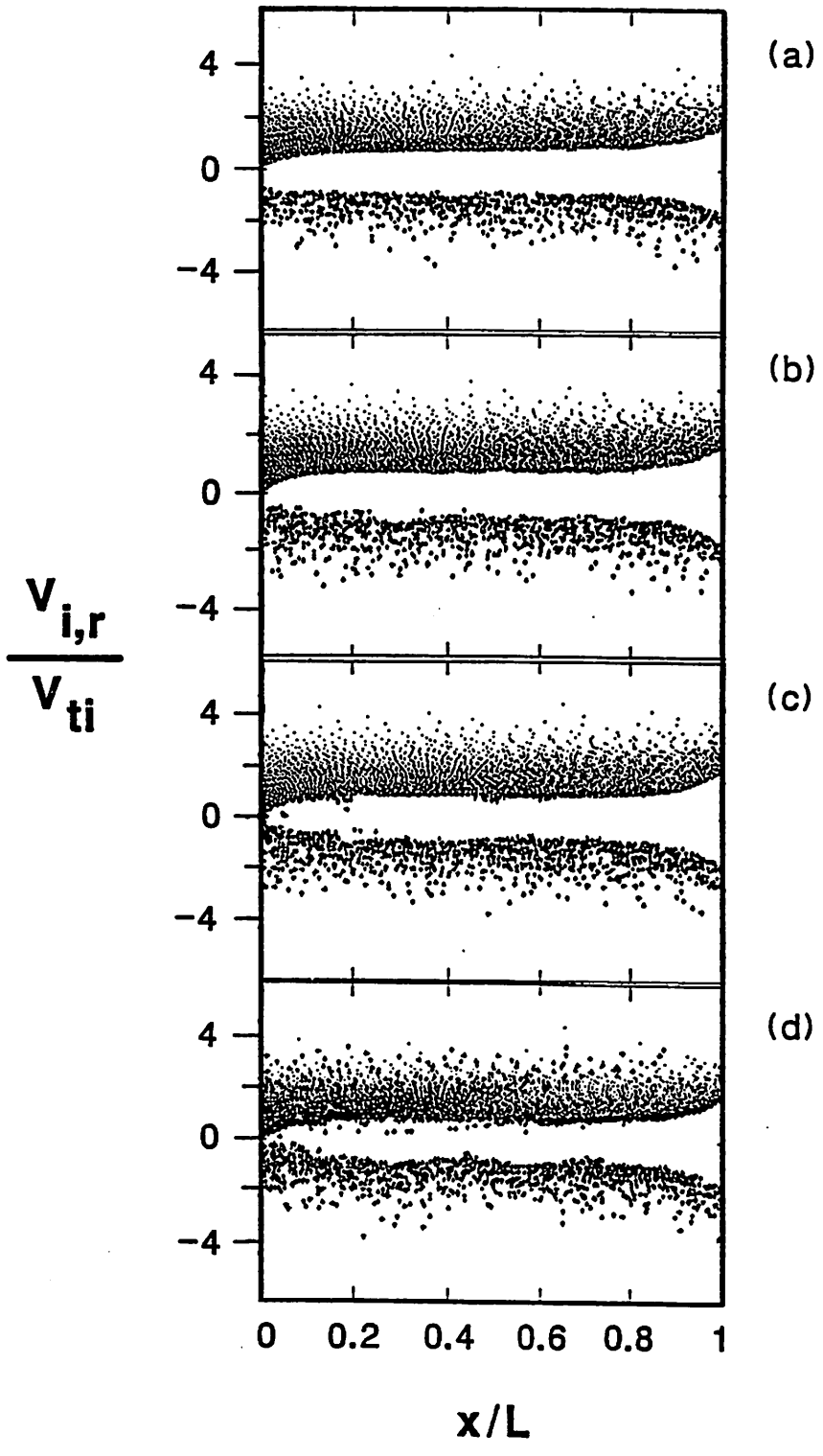

FIG. 9. Ion velocity scatter vs. distance at various times during the simulation run with $-V_r/V_i = 1$ for an ion reflection coefficient of 0.2, $M/m = 40$, and $T_{Si}/T_{Se} = 1$. Simulation snapshots are at times of 15.6, 23.4, 31.2, and 62.5 L/V_{te} from the top to bottom figures. The system length L is $27\,\lambda_D$. Primary ions (dots) have positive velocities and reflected ions (plusses) have mostly negative velocities.

Hence, these slow reflected ions arrive at the source plane with extra energy instead of zero energy.

After two transit times for slower ions ($\approx 12\,L/V_{te}$) beyond the equilibration time for ψ_C in Fig. 8(a), the primary and reflected ion streams interact as seen in Figs. 9(b)–9(d). At $t=23.4$ in Fig. 9(b), the reflected ion stream indicates increased fluctuations. At $t=31.2$ in Fig. 9(c), some reflected ions have been repelled by waves in the potential profile prior to reaching the source plane. Thus some reflected ions have a positive velocity. At $t=62.5$ (the final simulation time) in Fig.9(d), an even greater number of reflected ions have positive velocities; however, the two-stream interaction has either insufficient strength or too great a wavelength relative to L to cause both streams to merge toward a zero velocity.

To better understand the two-stream interaction for $\alpha=1$, the simulation parameters of length L and reflection coefficient ζ are varied. The simulation described in the above paragraph has length $L=27\lambda_D$ at the final time step; 128 grid cells are used to discretize the region. To simulate a region which has the same grid spacing and λ_D resolution but twice the length, then the injected flux F is doubled and 256 grid cells are used. Then twice the number of time steps are required to reach $\partial N/\partial t=0$. Even with this long simulation region, the two ion streams remain separate with a few trapped reflected ions near zero velocity. However, for $\zeta=0.4$ or 0.6, the streams interact strongly. Vortices are seen in the ion scatter plots and the streams separate periodically in time and space. Unlike the earlier case for $\zeta=0.2$, a final configuration of ions in velocity space is not attained during the time of particle equilibration. This strong interaction enhances fluctuations at the collector of potential and kinetic energy flux (discussed in the next section). Consequently, the reflected ion density increases with ζ which creates a stronger two-stream interaction which has a characteristic wavelength less than the system length of about

$40\lambda_D$. Details of the simulations with $\zeta = 0.4$ and 0.6 are not shown here because $\zeta < 0.2$ is more realistic from a materials consideration.

Allowing a fraction of reflection energy to be absorbed by collector atoms causes the primary and reflected ion streams to merge as seen in Figs. 10(a)–10(d). The times of the snapshots of ion scatter plots for $\alpha = 0.9$ are the same as those of the snapshots in Figs. 9(a)–9(d). At $t = 15.6$ in Fig. 10(a), both streams appear the same as those in Fig. 9(a) because the earlier potential values for $\alpha = 1$ and $\alpha = 0.9$ in Figs. 8(a) and 8(b) are the same. At $t = 23.4$ in Fig. 10(b) and at $t = 31.2$ in Fig. 10(c), the two streams begin to lose energy and merge. At these times, the value of ψ_P is almost zero as seen in the potential history in Fig. 8(b). At $t = 62.5$ in Fig. 10(d), both streams have lost sufficient energy such that the minimum ion speed in the center of the region is zero. This same sequence of events is observed for $\zeta = 0.4$ and 0.6 with $\alpha = 0.9$. The final configuration of the ions in velocity space for both cases is the same as in Fig. 10(b) except for the difference caused by differing values of ψ_C.

2. *Spatial profiles at steady state*

a. Steady state defined. The actual ratio of reflected/incident ion fluxes at the collector reaches ζ within a few tens of time steps from $t = 0$ because only a few particles are injected into the system during one time step. Generally, the collector potential equilibrates in 3.2 transit times of an ion traveling with the velocity of $V_{te}[2\mu\tau(\pi^{-1} - \psi_C/\tau)]^{1/2}$ as observed in Fig. 8 for $\zeta = 0.2$ with $\alpha = 1$ and 0.9. (This expression for equilibration time is the same observed in the previous paper[6] for $\zeta = 0$.) By this time of potential equilibration, the ion and electron fluxes are spatially equal and the net collector current is zero. However, the individual fluxes are not constant in space; i.e. the injected electron flux F is greater than the electron flux reaching the collector. The fluxes become spatially constant in approximately

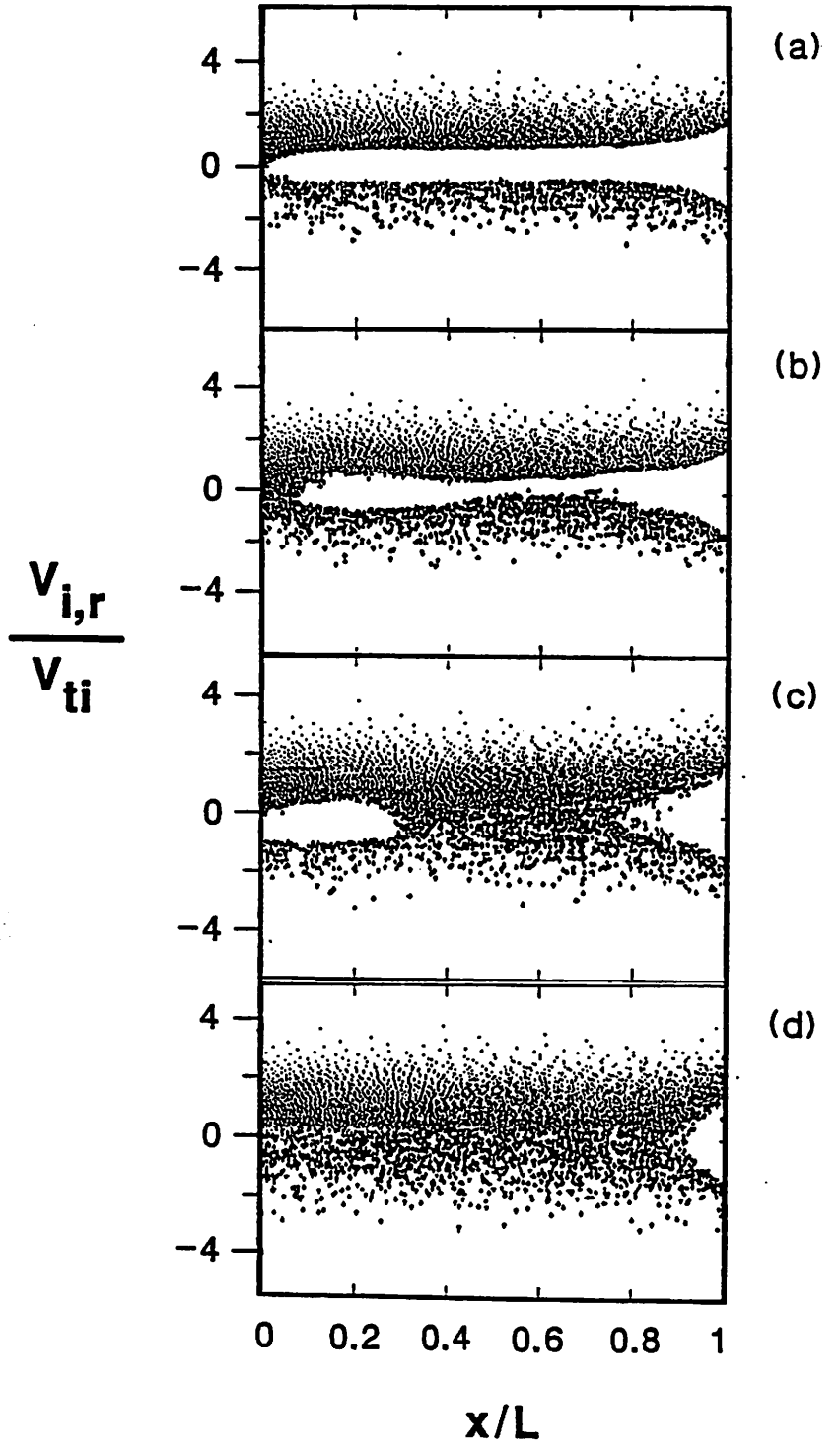

FIG. 10. Ion velocity scatter vs. distance at various times during the simulation run with $-V_r/V_i = 0.9$ for an ion reflection coefficient of 0.2, $M/m = 40$, and $T_{Si}/T_{Se} = 1$. Simulation times are 15.6, 23.4, 31.2, and 62.5 L/V_{te} from the top to bottom figures. The system length L is $27\lambda_D$. Primary ions (dots) have positive velocities and reflected ions (plusses) have mostly negative velocities.

twenty times $L(-\psi_C)^{-1/2}V_{te}^{-1}$. At this same time, by conservation of particles, the total number of system particles becomes temporally constant. All steady state plots shown hereafter are calculated at a time after particle equilibration with the exception of the case for $\zeta = 0.6$ for $\alpha = 1$ and 0.9. (For such a large value of ζ, the value of ψ_C requires an inordinate amount (several hours) of Cray computation time to reach the time for particle equilibration.)

b. Electrostatic potential. For simulation with $\alpha = 1$ and reflection coefficients of 0.2, 0.4, and 0.6 the final values of ψ_C and ψ_P show good aggreement with theory. These simulation results for $\alpha = 1$, represented by circles, are plotted in Fig. 4 to compare with the full kinetic theory for $\psi_C(M/m, \tau, \zeta)$ and $\psi_P(M/m, \tau, \zeta)$. The bars around each data point indicate the oscillation amplitude for each measurement of ψ_C and ψ_P. Fluctuations in potential increase substantially with ζ. For $\zeta = 0.4$, the number of particle electrons per λ_D is $N_D \approx 300$ which causes the magnitude of the oscillation amplitudes shown in Fig. 4. For $\zeta = 0.6$, these large fluctuations are caused in part because $N_D \approx 400$ but also are enhanced by the strong interaction between the primary and reflected ion streams discussed in Sec. III C 1 b.

For simulation with $\alpha = 0.9$ and reflection coefficients of 0.2, 0.4, and 0.6 the final values of $-\psi_C$ and $-\psi_P$ fall below theory for $\alpha = 1$. These simulation results for $\alpha = 0.9$, represented by squares, are plotted in Fig. 4. For each run with $\alpha = 0.9$, the source sheath potential drop is almost zero. Oscillations in potential increase substantially with ζ and are comparable to those for $\alpha = 1$.

In particular for $\mu = 1/40$, $\tau = 1$, and $\zeta = 0.2$, the value of $\alpha = 0.986$, derived in Sec. II F 1, is the minimum α which allows Eqs. (11) and (12) to be solved and provides the solution of $\psi_C = -1.38$ and $\psi_P = -0.18$. From simulation with $\zeta = 0.2$ and $\alpha = 0.9$, then $\psi_C = -1.41 \pm 0.07$ and $\psi_P = -0.02 \pm 0.05$. Hence, the solution of minimum α does not provide the same answers for ψ_C and ψ_P when the velocity

reflection coeffient α is less than that value, i.e. then the monotonically decreasing solution for potential is not valid.

The electrostatic potential profiles shown in Fig. 11 are generated via particle simulation for $\alpha = 1$ and $\alpha = 0.9$ using $\mu = 1/40$, $\tau = 1$, and $\zeta = 0.2$ Each case has system length of 27 and $30\,\lambda_D$, respectively. With the same injected flux F, the case of $\alpha = 0.9$ results in a greater overall plasma density. Generally with $\alpha = 0.9$, because more reflected ions have insufficient energy to traverse the system, their mean velocity is reduced and so their density increases by flux conversation. Hence, as these ions stop to converse and exchange energy, they attract attention and cause an increase in density. This increased ion density reduces the overall potential curvature, $\nabla^2\psi$, according to Poisson's equation, which reduces $-\psi_C$. At this last simulation time of $t = 62.5$, these potential profiles do not decrease monotonically even though the time-averaged potential profiles do.

c. Velocity distributions. The velocity distributions of primary and reflected ions and electrons for the simulation parameters of $\mu = 1/40$, $\tau = 1$, $\zeta = 0.2$, and $\alpha = 0.9$ are shown in Fig. 12. These distributions correspond to the potential profile in Fig. 11 for $\alpha = 0.9$ and have been evaluated over central region from the scatter plot (shown in Fig. 10(d) for the ions) spatially averaged from $x/L = 0.25$ to 0.75. The number of particles at each discrete value of velocity, i.e. $f(v)$, is evaluated from the velocity scatter at each gridpoint and then spatially averaged over the grids corresponding to $0.25 \leq x/L \leq 0.75$. The distribution $f(v)$ at each discrete value of x is weighted and summed over all velocities for each species to provide the various profiles such as temperature and energy flux.

The velocity distributions shown in Fig. 12 are predictable for primary ions, f_i, and electrons, f_e, with the potential profile in Fig. 10 for $\alpha = 0.9$. However, the velocity distribution of reflected ions, f_r, spilling into positive velocity space, is not

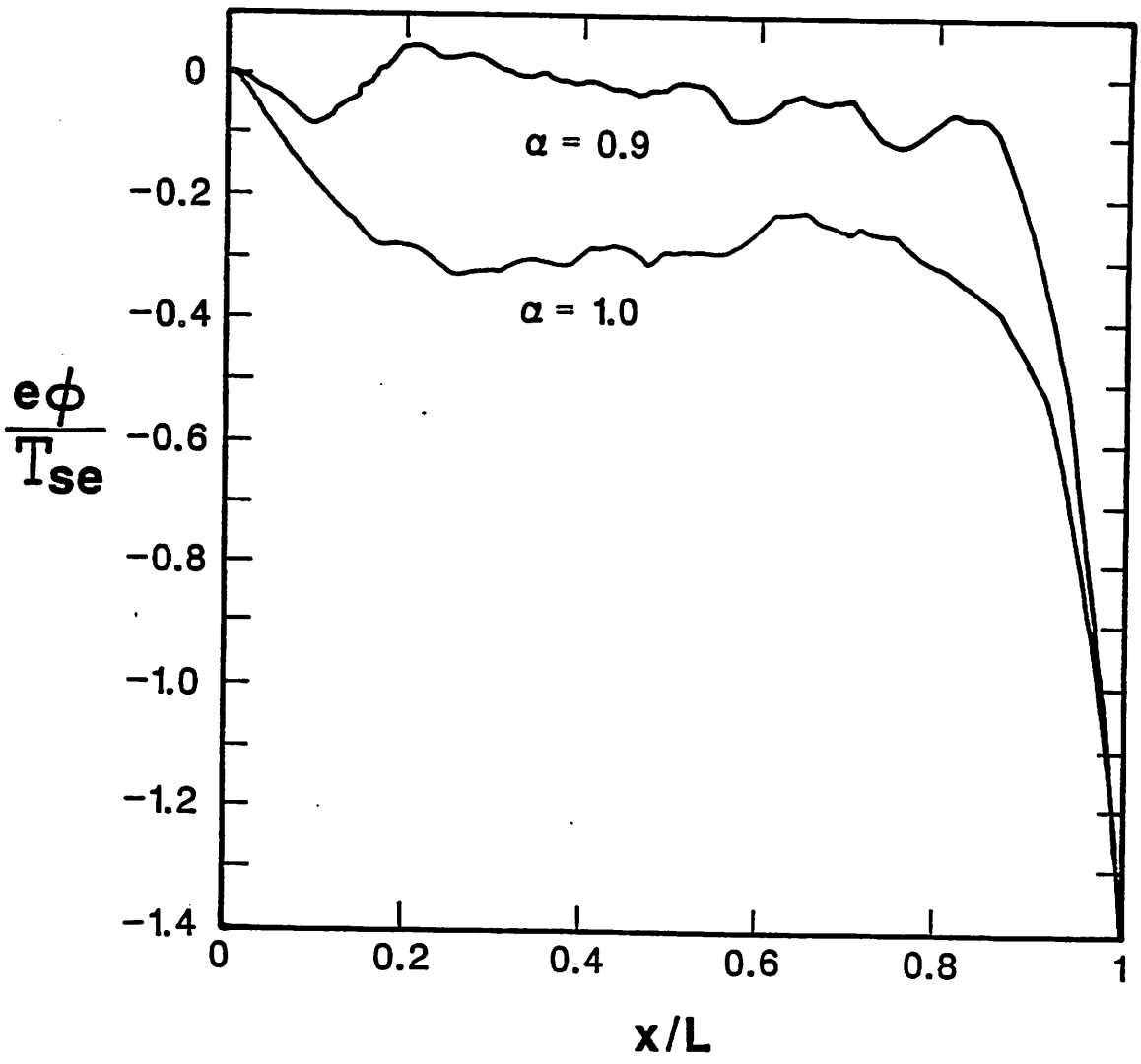

FIG. 11. Potential profiles from simulation for 2 values of reflected velocity, $\alpha = -V_r/V_i$, with an ion reflection coefficient of $\zeta = 0.2$, $M/m = 40$, and $T_{Si}/T_{Se} = 1$. The system lengths L are $27\lambda_D$ for $\alpha = 1$ and $30\lambda_D$ for $\alpha = 0.9$. Both are snapshots at the last time of 62.5 L/V_{te}. The potentials are normalized as $\psi = e\phi/T_{Se}$.

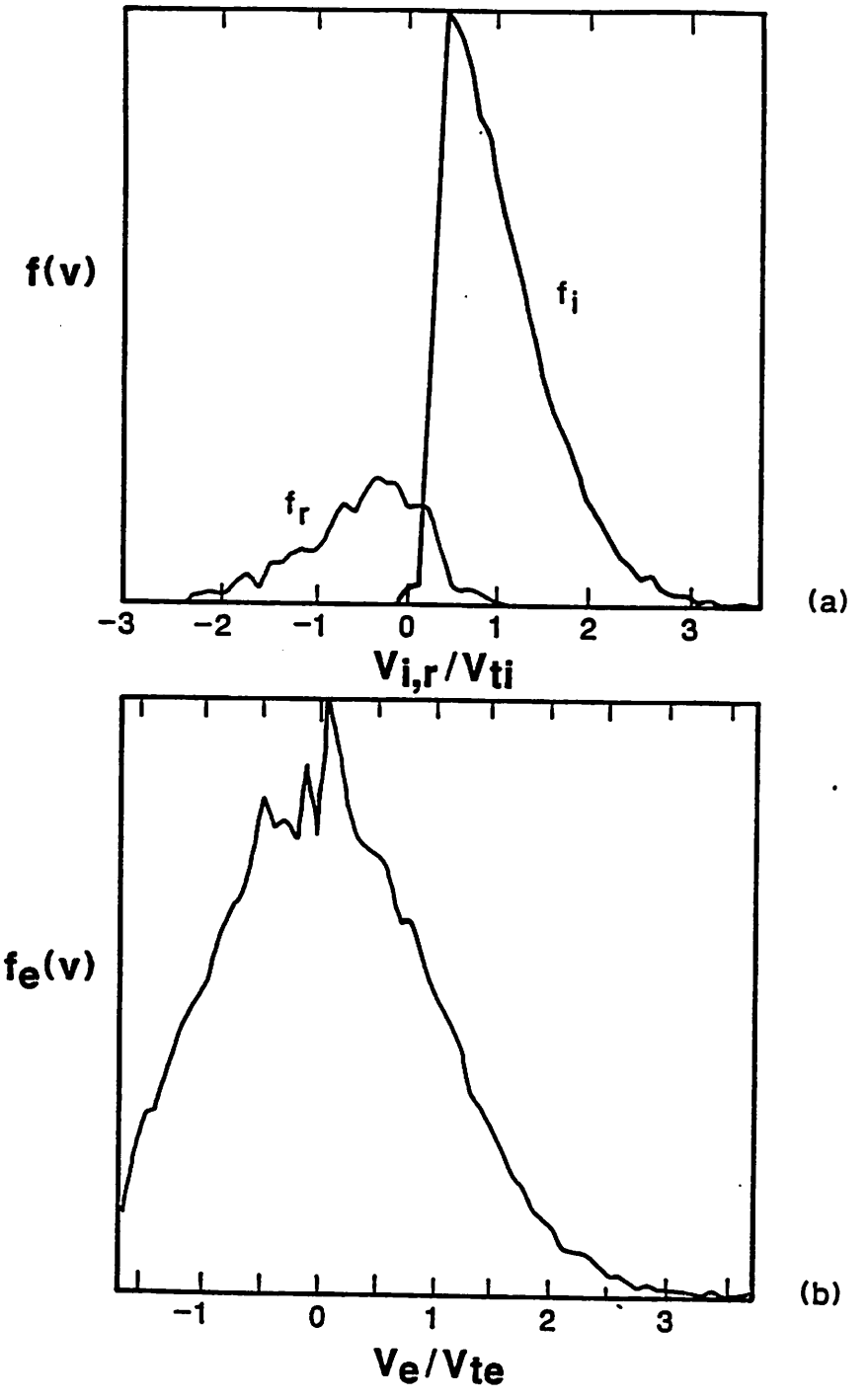

FIG. 12. Velocity distributions for (a) primary, f_i, and reflected, f_r, ions and (b) electrons, f_e. Distributions are averaged spatially over the simulation from $x/L=0.25$ to 0.75 at a time of 62.5 L/V_{te}. Simulation parameters are $-V_r/V_i=0.9$, ion reflection coefficient of 0.2, $M/m = 40$, and $T_{Si}/T_{Se} = 1$. Ion and electron velocities are normalized respectively to the ion and electron thermal velocities V_{ti} and V_{te} at the source.

predictable with this same potential profile. Most of the potential in the central region of $0.25 \leq x/L \leq 0.75$ is nearly zero. Thus according to energy conservation, the absolute value of minimum velocity for primary ions is zero; the minimum observed in Fig. 12(a) is very near zero as predicted. Contrarily for reflected ions, the equation for minimum velocity V_{Mr} in Eq. (1) provides no real solution for V_{Mr} when $\alpha = 1$ and $\psi = 0$. Observed in Fig. 11, the waves in the potential profile which cause $\psi > 0$ give some of the reflected ions sufficient energy to attain positive velocity, as is seen in f_r of Fig. 12(a). For the electron distribution in Fig. 12(b), $f_e(v)$ exhibits the cut-off Maxwellian shape with the most number of electrons near zero. By energy conservation, the minimum electron velocity, $V_{Me} = V_{te}(2\psi - 2\psi_C)^{1/2}$. Hence for $\psi = 0$ in this simulation, $V_{Me} = 1.67\, V_{te}$ which is observed in Fig. 12(b).

d. Ion temperatures. A comparison of theoretical and simulation results for the effective temperature profiles of primary and reflected ions, $T_i(x)$ and $T_r(x)$, normalized to the ion source temperature, τT_{Se}, are shown in Fig. 13. The temperature profiles generated via simulation are found in evaluating the mean square deviation of the velocity about the mean which has been time-averaged over a plasma period prior to the last time step. The ion scatter plot in Fig. 10(d) is the last used for the averaging period to determine $T_i(x)$ and $T_r(x)$ in the solid curves of Fig. 13. The dashed lines indicating theory results are generated using the potential profile in Fig. 11 for $\alpha = 0.9$ and the expressions for $T_i(\psi)$ in Eq. (14) of the previous paper[6] and $T_r(\psi)$ in Eq. (7) of the present paper.

The theoretical and simulation results in Fig. 13 show good agreement for $T_i(x)$ and $T_r(x)$ which indicates no additional thermal spreading of the two ion streams not accounted for by energy conservation (which assumes $\partial/\partial t = 0$). When $\psi(x) > 0$ (in Fig. 11), the expression for $T_i(\psi)$ cannot be evaluated; then, $\psi = 0$ is assumed. Hence near $x/L = 0.25$, T_i (dashed line in Fig. 13(a)) is a constant

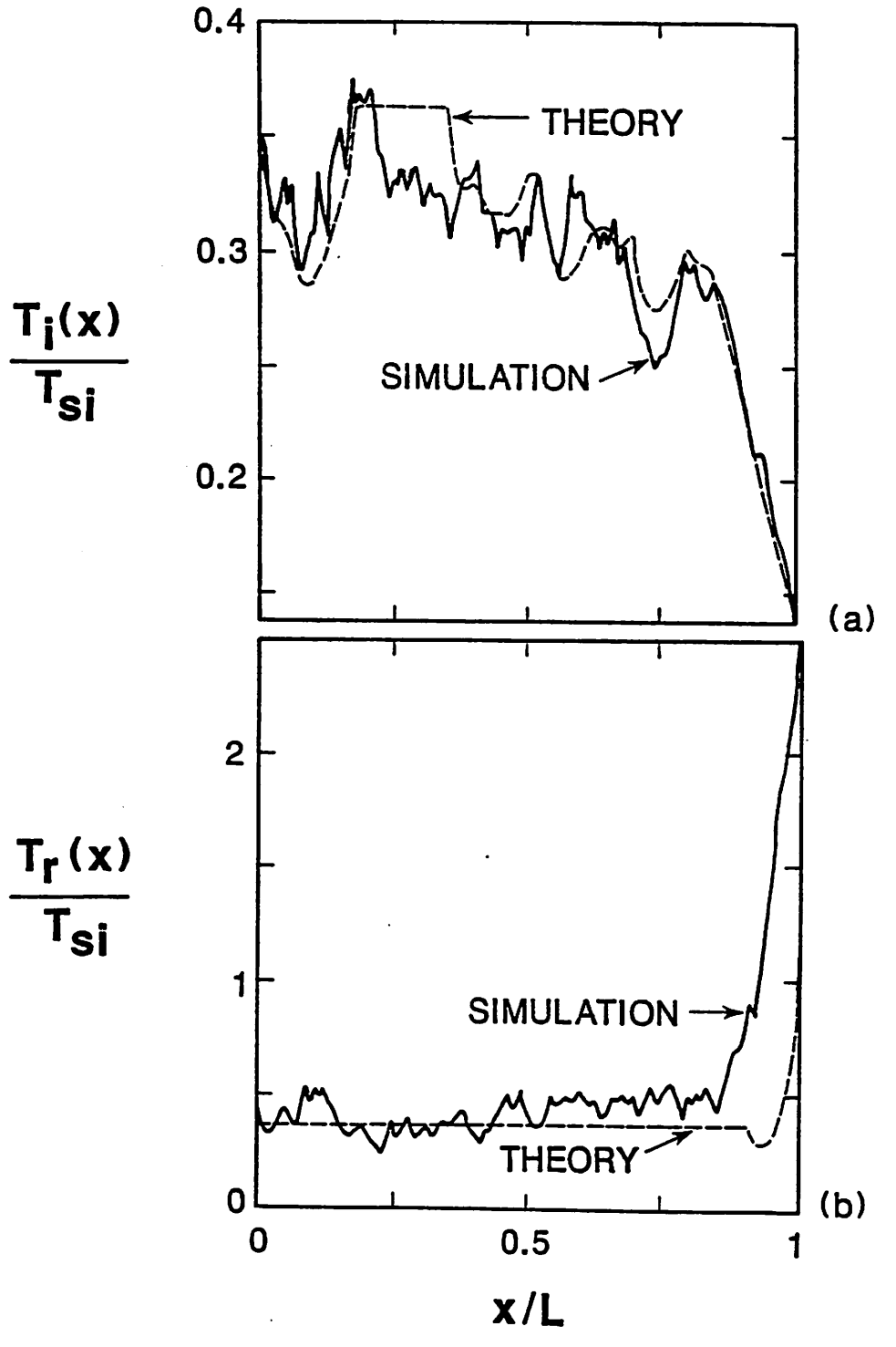

FIG. 13. Primary ion temperature T_i and reflected ion temperature T_r spatial profiles generated with $-V_r/V_i = 0.9$, ion reflection coefficient of 0.2, $M/m = 40$, and $T_{Si}/T_{Se} = 1$. Solid line indicates simulation results. Dashed line indicates theory determined using $\psi(x)$ as obtained from simulation in Fig. 11.

which equals $1-2\pi^{-1}$. Similarly, when $\psi > \psi_C(1-\alpha^2)$, the expression for $T_r(\psi)$ cannot be evaluated; then, $\psi = \psi_C(1-\alpha^2)$, i.e. $V_{Mr}=0$ (from Eq. (1)), is assumed. Hence for $x/L<0.9$, T_r (dashed line in Fig. 13(b)) is also the constant 0.36. Despite these approximations for $T_i(x)$ and $T_r(x)$, the theory closely predicts the simulation profiles.

The largest difference between the theory and simulation for $T_r(\psi)$, shown in Fig. 13(b), occurs in the collector sheath. A closer view of the velocity scatter in Fig. 10(d) reveals that some reflected ions are repelled by the potential and return to $x=L$. These repelled reflected ions have insufficient energy to move beyond the collector sheath because of the energy lost to the collector with $\alpha=0.9$. The reflected ions actually have a decelerated distribution for negative velocities along with an accelerated distribution for positive velocities. Because the positive velocities cause an increased deviation about the mean velocity, $T_r(\psi)$ from simulation lies above that from theory (which considers only the decelerated, negative velocities).

e. Kinetic energy fluxes for ions. The theoretical and simulation results in Fig. 14 show good agreement for $Q_i(x)$ and $Q_r(x)$ which indicates no change in total energy of the two ion streams not accounted for by energy conservation. These plots for $Q_i(x)$ and $Q_r(x)$ divided by FT_{Se}, are also that for energy transmission factor $\delta_i(\psi)$ and $\delta_r(\psi)$. The kinetic energy flux profiles generated via simulation are found in evaluating the third velocity moment which has been time-averaged over a plasma period prior to the last time step. The ion scatter plot in Fig. 10(d) is the last used for the averaging period to determine $Q_i(x)$ and $Q_r(x)$ in the solid curves of Fig. 14. The dashed lines indicating theory results are generated using the potential profile in Fig. 11 for $\alpha=0.9$ and the expressions for $\delta_i(\psi)$ and $\delta r(\psi)$ derived in Sec. II B 3. Because these derivations use the assumption of a monotonically decreasing potential profile, whenever $\psi>0$ then $\psi=0$ is used in both expressions.

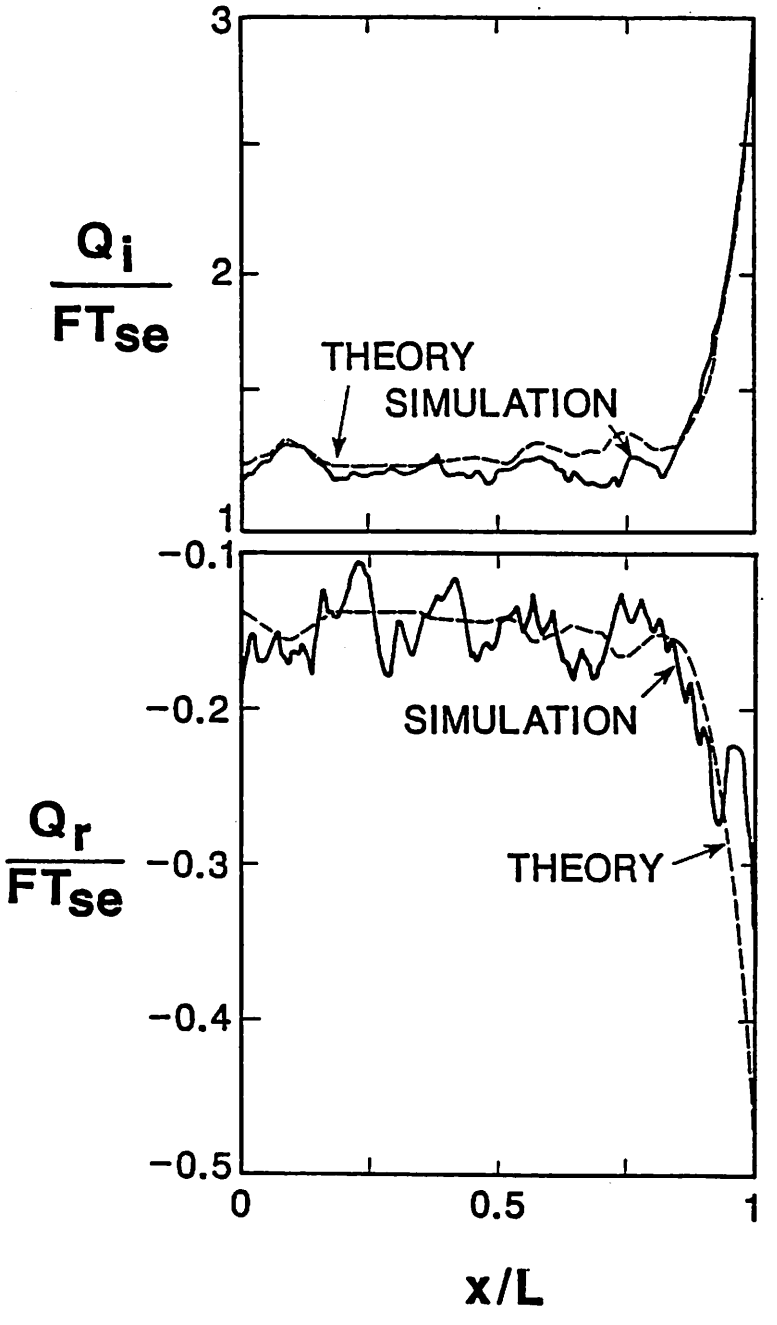

FIG. 14. Kinetic energy flux profiles for primary ions, Q_i, and reflected ions, Q_r, generated with $-V_r/V_i = 0.9$, ion reflection coefficient of 0.2, $M/m = 40$, and $T_{Si}/T_{Se} = 1$. Solid line indicates simulation results with one-dimension in velocity. Dashed line indicates theory determined with $\psi(x)$ from simulation in Fig. 11. Profiles are divided by electron flux F and electron source temperature T_{Se}.

Again, the largest difference between the theory and simulation in Fig. 14 occurs in the collector sheath for Q_r for the same reasons described above for T_r.

3. *Energies at the collector at steady state*

a. Kinetic energy flux. The history of kinetic energy flux at the collector, $Q(\psi_C)$, is evaluated with the velocity distribution of the number of particles passing $x = L$ in each time step. This velocity distribution of current, $vf(v)$, times v^2 determines $v^3 f(v)$ which is integrated over all incident velocities to find $Q(\psi_C)$. For $\zeta = 0.2$, 0.4, and 0.6 with $\alpha = 1$ and 0.9, the simulation results in one-dimension (1-d) are adjusted to three-dimensions (3-d) to compare with theory. The two transverse direction in velocity space are assumed to have full-Maxwellian velocity distributions. The contribution by each dimension to Q_α is $T_{S\alpha}F_\alpha$ where α represents each species. Thus, the normalized contribution from the transverse directions, $(\tau-\zeta\alpha^2\tau+1-\zeta)/(1-\zeta)$, is added to the total energy transport coefficient, $\delta_T = Q_T/(FT_{Se})$, from the 1-d simulation results. Corrected to 3-d, these simulation results with $\alpha = 1$, indicated with circles, and $\alpha = 0.9$, indicated with squares, are shown in Fig. 6 with the theory from Eq. (10) at $\mu = 1/40$ for $\tau = 1$ with $\alpha = 1$. The bars on each data point indicate the oscillation amplitude in δ_T even after the history values are time-averaged over a plasma period. The persistence of these averaged oscillations indicate fluctuations occuring with longer periods.

Fluctuations in collector potential cause half of the amplitude of the large fluctuations in δ_T seen in Fig. 6. For example, with $\zeta = 0.4$ and $\alpha = 1$ from Fig. 4, $\psi_C = -1.8 \pm 0.12$. Substituting these parameters into Eq. (10) provides $\delta_T(\zeta) = 4 - \psi_C$. With $\delta_T(0) = 5.04$ from simulation with $\zeta = 0$, then the normalized δ_T fluctuates ± 0.024; whereas, the fluctuation level measured via simulation is ± 0.06 as shown in Fig. 6. Consequently, increasing with ζ, the remaining fluctuation level appears to be caused somewhat by the two-stream interaction. This claim is

guarded because the fluctuations in δ_T is the same at each ζ when $\alpha=1$ or $\alpha=0.9$. One would expect the strong two-stream interaction observed with $\alpha=1$ to have larger fluctuations than the relatively quiet equilibrated state of the ion velocity distribution with $\alpha=0.9$. Thus the additional amplitude of oscillations appear to be caused by something as yet to be explained.

For $\zeta \leq 0.4$ and $\alpha = 1$, the comparison of theoretical and simulation results indicate good agreement in Fig. 6. Although as ζ is raised, the simulation data occur increasingly below theory. As described in Sec. III C 1 b for $\zeta = 0.4$ and 0.6, the two ion streams fluctuate considerably in velocity space. Because some of the ions in these streams often reach zero velocity, these fluctuations tend to reduce the mean energy carried by the ions reaching the collector. However, the reflected ions generated at the collector also have a reduced departure energy which should balance the effect of reduced incident energy. Thus the two-stream interaction also does not seem to explain the increased discrepancy between theory and simulation.

The following are a few more possible causes of the increased discrepancy between the theory and simulation in Fig. 6 for $\alpha=1$. In the simulation for $\zeta \leq 0.4$, the contribution to δ_T by the electrons, δ_e, is the value predicted theoretically so that electron behavior also does not cause the increased discrepancy. Finally, the simulation results for δ_T are time-averaged over a plasma period. Within this time of about 100 time steps the actual reflected ion flux lags behind the value of $-\zeta F_i$ by at most ten time steps. Hence, the reflection technique also does not seem to cause the discrepancy for plasma effects with a characteristic time greater than a plasma period.

The existence of self-induced fluctuations is not precluded. For example with $\alpha=0.9$, the low energy reflected ions are repelled by the collector sheath, as shown in Fig. 10(d). These ions return to the collector with their initial low energy and

generate more reflected ions with even lower energy. (Somehow this mechanism reaches a steady state.) In this way, reflected ions may arrive in bunches rather than continuously which would cause increased oscillations of kinetic energy flux at the collector.

For the particular case of $\zeta = 0.6$, the total number of particles in the system continues to grow, as mentioned in Sec. III C 2 a. Thus a greater electron density would increase the electron flux up to F which raises the kinetic energy flux at the collector. Recall that the kinetic energy flux is the mean kinetic energy per particle times the particle flux.

Simulation results, using $\zeta \leq 0.4$ and $\alpha = 0.9$, occur above theoretical results using $\tau = 1$ with $\alpha = 1$, as seen in Fig. 6. Again, the case of $\zeta = 0.6$ shows the largest discrepancy because the total number of particles in the system did not equilibrate. Initially one might predict that δ_T results for $\alpha = 0.9$ would occur below theory because of the decreased ψ_C (seen in Fig. 4 at each ζ). The following effect overcompensates for the decreased ψ_C and causes a net increase in δ_T as α is varied from 1 to 0.9. The net (total) energy flux carried to the collector is greater when the collector absorbs a fraction $(1 - \alpha^2)$ of the reflection energy because the energy removed by the reflected ion flux is less. When $\alpha = 1$, the energy removed by the reflected ion flux balances the energy added by the additional incident flux of primary ions; where "additional" refers to reflected ions which are refluxed and become primary ions. (With $\tau = 1$ and $\alpha = 1$ applied to Eq. (10), then $\delta_T = 4 - \psi_C$ i.e. no ζ dependence exists.)

b. Mean kinetic energy of primary ions. The technique described above for evaluating kinetic energy flux at $x = L$ in the simulation is also used to evaluate mean kinetic energy. Defined in Sec. II F 2, mean kinetic energy, $W = F_i Q_i(\psi_C)$. Thus in the simulation, $Q_i(\psi_C)$ is evaluated and then multiplied by $(1 - \zeta)/F$ to

find W. Adding τT_{Se} to these 1-d simulation results for W adjusts the data to compare with the 3-d theory which is $W = T_{Se}(2\tau - \psi_C)$ from Eq. 8. Data using $\zeta = 0.2$, 0.4, and 0.6 for $\alpha = 1$ are indicated by circles and for $\alpha = 0.9$ by squares is compared with theory in Fig. 7. The bars on each data point indicate the oscillation amplitude in δ_T even after the history values are time-averaged over a plasma period.

Theoretical results for $\tau = 1$ and $\alpha = 1$ consistently overpredict W measured from simulation for both $\alpha = 1$ and $\alpha = 0.9$ as seen in Fig. 7. For mean ion kinetic energy at the collector, the fluctuations and deviations from theory can be explained with the two-stream interaction. As discussed in the above subsection for $\alpha = 1$, the interaction between the primary and reflected ion streams is enhanced as ζ increases. Mean incident energy is reduced because the streams fluctuate and often reach zero velocity. Contrarily, time-independent kinetic theory predicts the streams should remain separate (as seen for $\zeta = 0.2$ in Fig. 10(d)) which generates a higher W. As expected and observed in Fig. 7, this deviation from theory and fluctuations increase with ζ.

Fluctuations in W are less for $\alpha = 0.9$ than for $\alpha = 1$ at each ζ shown in Fig. 7 (unlike fluctuations in δ_T). For each ζ, the final configuration of the ions is that shown in Fig. 10(d) so that only potential oscillations cause those observed in W. For example, with $\zeta = 0.4$ and $\alpha = 0.9$ from Fig. 4, $\psi_C = -1.69 \pm 0.09$. Using $W = T_{Se}(2 - \psi_C)$ and the normalization constant $W(0,1)$ of $3.04 T_{Se}$, then the normalized W fluctuates ± 0.03. Similarly for $\zeta = 0.2$ and 0.6, fluctuations are several times smaller than those predicted using ψ_C fluctuations. Hence, this quiet configuration of the ion streams seems to reduce oscillations in W. A similar calculation for each ζ with with $\alpha = 1$ predicts fluctuations in W from ψ_C oscillations that are comparable to those observed via simulation for W shown in Fig. 7.

The increased difference in W with ζ is caused partially by the reduction in ψ_C

not fully predicted by theory, as seen in Fig. 4. If the value of ψ_C from simulation is substituted into the above expression for W and normalized then the simulation results in Fig. 7 still overpredict W. For example with $\zeta = 0.4$ and $\alpha = 0.9$ (as above), then $W/W(0,1) = 1.21$, which lies considerably above the data point at 1.13. Again, the ion scatter plot in Fig. 10(d) reveals that slower reflected ions are repelled by the collector sheath, return to the collector, and a fraction of which generate even slower reflected ions. Not accounted for in the kinetic theory, this additional contribution of low energy reflected ions reduces the mean kinetic energy measured for all incident ions.

IV. COMPARISON WITH A PREVIOUS RESULT

Brooks[9] numerically solves time-independent Vlasov-Poisson equations to model boundary effects on the collector sheath region. Secondary electron emission combined with ion reflection at the boundary is studied for a D-T plasma with $T_{Si} = 0.25\,T_{Se}$. He studies the effect of ion reflection on the potential drop across the collector sheath, ϕ_F, by varying ζ from 0 to 0.15. Brooks does not derive an analytical expression so that our results can only be compared for a variable ion reflection coefficient with no electron emission at the above plasma parameters.

In detail, Brooks specifies boundary conditions at the entrance of the collector sheath region rather than at the plasma source. At the entrance to the collector sheath region, the ion kinetic energy equals the electron kinetic energy. At the plasma boundary, ion and electron densities and fluxes are equal. Here also each plasma species leaving the source and traveling toward the collector have a half-Maxwellian distribution. The Vlasov-Poisson equations for the distribution functions of primary and reflected ions and of primary and secondary electrons are solved numerically and iterated until the plasma boundary conditions are satisfied.

Brooks uses an ion reflection coefficient which is independent of incident ion energy as is ζ in my model. The velocity of reflected ions equals that of the incoming ions.

In contrast, my results show a somewhat larger increase in potential drop across the collector sheath than do the results of Brooks as the ion reflection coefficient is increased. From Fig. 3, collector sheath drop, $\psi_C - \psi_P$, is independent of τ for $\tau < 1$, and equals -2.98 for $M/m = 4590$ (the mean value of mass ratio for a D-T plasma). For $\zeta = 0.15$, then $\psi_C - \psi_P = -3.29$. In Brooks's Fig. 3, $e\phi_F/T_{Se}$ is shown as a function of the electron emission coefficient for ion reflection coefficients of $\zeta = 0$ and $\zeta = 0.15$. With no electron emission, $e\phi_F/T_{Se}$ equals approximately -3.05 for $\zeta = 0$ and -3.10 for $\zeta = 0.15$. Consequently, although, for $\zeta = 0$, both studies provide slightly different solutions, for $\zeta = 0.2$, my model predicts an increase in collector sheath potential drop that is six times larger than the increase predicted with the model of Brooks.

V. CONCLUSIONS

The effects of ion reflection on the plasma source and collector sheaths are analyzed for ion/electron mass ratios from 10 to 10^4 with ion/electron temperature ratios τ of 0.1, 1, and 10. Reflection with coefficients ζ up to 0.6 at the electrically floating collector is simulated for a mass ratio of 40 with $\tau = 1$ for reflected ions having a reflected/incident velocity ratio α of 1 and 0.9. Density, drift velocity, temperature, kinetic energy flux, and heat flux for all three species are derived at values of potential at the collector and across the source sheath.

For all of the above values, good agreement exists between our electrostatic particle simulation and the fully kinetic model for $\zeta < 0.2$. At larger ζ with $\alpha = 1$, the increased interaction between the primary and reflected ion streams causes greater fluctuations in potential but without affecting the time-averaged value of

ψ_C. However, these fluctuations reduce the mean kinetic energy of ions reaching the collector to below that predicted theoretically. For $\alpha = 0.9$, potential does not decrease monotonically so that the present kinetic theory cannot exactly model the resultant potential profile but can provide an increased understanding on the effect of reflection energy lost to the collector on the sheath region. Observed via simulation, this effect of slightly reducing the energy of reflected ions generates a strong two-stream interaction which then causes the two ion streams to overlap in velocity space and the potential drop across the source sheath to fall to zero. Compared to $\alpha = 1$ at the same values of ζ, this merging of streams causes a slight decrease in ψ_C, an increase in energy transported to the collector, and a substantial reduction in the mean kinetic energy of ions reaching the collector.

For a D-T plasma with $T_{Si} = T_{Se}$ and $\alpha = 1$, increasing the ion reflection coefficient from 0 to 0.2 causes the collector potential to change from -3.3 to -3.7, and both the total energy flux to the collector surface and the mean kinetic energy of incident ions to increase only by factors of 1.06 and 1.08, respectively. Allowing the collector surface to absorb a fraction of the incident ion energy during a reflection event may cause small changes to these macroscopic trends. Although with $\alpha < 1$, the shape and behavior of the potential profile is observed via simulation for $M/m = 40$ to change substantially, relative to $\alpha = 1$. The above trends in ψ_C for $\alpha = 1$ can also be accurately predicted with the simple analysis given in Eq. (28) only for $\tau = 1$. In summary, the simulation model provides substantial insight into the effect of the two-stream interaction on the potential profile and energy transport in the sheath region, the details of which are difficult to model near a boundary.

Acknowledgments

Special thanks is given to W. S. Lawson who contributed to the ideas on the algorithm developed for the energy conserving reflection. This research was sponsored by the U. S. Department of Energy under Contract DE-FG03-86ER53220.

APPENDIX: ENERGY CONSERVING REFLECTION

The simulation of ion reflection off a boundary having a large electric field requires an accurate formulation of the algorithm which governs the motion of the reflected particle after the reflection event. For the particular case of the boundary material composed of atoms with an infinite mass relative to the incident particles, energy must be conserved during the reflection event. Energy conservation at reflection is crucial in a steady state system, when particles are injected at a source, traverse a potential path, perfectly reflect at a boundary, and must return to the origination point. In this scenario, these particles should have no gain or loss in energy. In a real model, some of the energy of the reflected particle is imparted to the atoms in the boundary material. Hence, this exercise is provided as a reference for these cases.

During one time step of the simulation, a particle reaching the boundary also passes beyond it. The penetration depth depends on the previous location and present velocity of the particle. This velocity is determined with a leap-frog mover[10] at one-half time step earlier. On reflection, the position of the particle is mirrored back through the boundary. As a first guess, the new velocity is assigned the same magnitude but opposite sign of the old velocity. This method does not conserve energy because the particle has been reflected across a potential difference. The following derivation provides a correction in this simply reflected velocity which includes the effect of the potential change and a one-half time step correction.

A particle of mass m, charge q, and velocity v moving along x in a time-independent electric field E has constant energy $\mathcal{E}$,

$$\mathcal{E} = \frac{mv^2}{2} - qEx. \qquad (A.1)$$

The acceleration a on the particle is

$$a = E\left(\frac{q}{m}\right). \tag{A.2}$$

This acceleration is assumed to be constant within one grid cell width Δx from the boundary and over one time step Δt prior to reflection.

The simulation provides x_p and $v_{p-\frac{1}{2}}$, where the subscript p denotes the time step prior to boundary penetration. At the next time step when the particle is moved, the new velocity and position become

$$v_{p+\frac{1}{2}} = v_{p-\frac{1}{2}} + a\Delta t \tag{A.3}$$

and

$$x_{p+1} = x_p + v_{p+\frac{1}{2}}\Delta t. \tag{A.4}$$

If x_{p+1} exceeds the system length L and the particle is reflected (as opposed to added to the boundary surface charge), then the new position and velocity are $\bar{x}_{p+1}$ and $\bar{v}_{p+\frac{1}{2}}$. The particle is repositioned from the boundary at the distance it would have penetrated the boundary. (This technique is discussed in Birdsall and Langdon.[10]) As illustrated in Fig. 15, this new position becomes

$$\bar{x}_{p+1} = 2L - x_{p+1}. \tag{A.5}$$

The simple velocity is then corrected to conserve energy. (Note that this simple velocity could have been used and then the particle position in Eq. (A.5) would have to be adjusted to conserve energy.) The particle, first accelerated by E at the boundary to x_{p+1}, is now decelerated by the same E to $\bar{x}_{p+1}$. The simple velocity is corrected with δ, where

$$\bar{v}_{p+\frac{1}{2}} = -v_{p+\frac{1}{2}} + \delta. \tag{A.6}$$

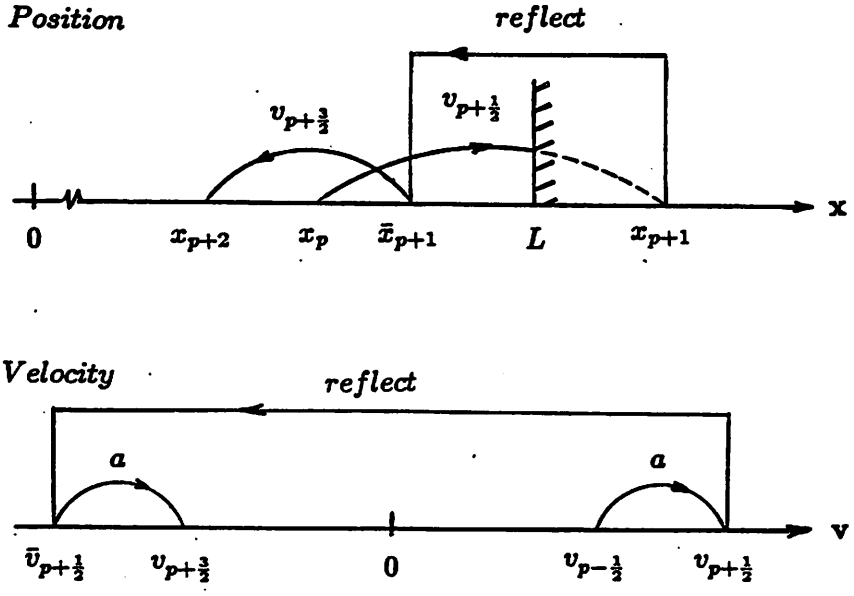

FIG. 15. Position and velocity of an ion before, during, and after reflection using the energy conserving reflection algorithm.

Equating $\mathcal{E}_p$ with $\mathcal{E}_{p+1}$ determines the value for $\bar{v}_{p+\frac{1}{2}}$. This energy balance gives

$$\frac{v_p^2}{2} - ax_p = \frac{\bar{v}_{p+1}^2}{2} - a\bar{x}_{p+1}. \tag{A.7}$$

Second-order approximations for v^2 at the full time step are

$$v_p^2 = v_{p+\frac{1}{2}} v_{p-\frac{1}{2}} \tag{A.8}$$

and

$$\bar{v}_{p+1}^2 = v_{p+\frac{3}{2}} \bar{v}_{p+\frac{1}{2}}. \tag{A.9}$$

The next velocity depends on the reflected velocity by

$$v_{p+\frac{3}{2}} = \bar{v}_{p+\frac{1}{2}} + a\Delta t. \tag{A.10}$$

Finally, Eqs. (A.3)–(A.6) and Eqs. (A.8)–(A.10) are substituted into the energy balance of Eq. (A.7). The solution for δ from this energy balance is in the quadratic equation:

$$0 = \delta^2 + \delta\left(a\Delta t - 2v_{p+\frac{1}{2}}\right) + 4a\left(x_{p+1} - L\right) - 2av_{p+\frac{1}{2}}\Delta t. \tag{A.11}$$

The ordering of terms in Eq. (A.11) determines the expression for δ. Because the leap-frog mover estimates position and velocity through a first-order central difference, these approximations (Eqs. (A.3), (A.4), and (A.10)) are of $O\left((\Delta t)^3\right)$. (Details of the ordering of the central difference equations are discussed in Botha and Pinder.[12]) Simple reflected velocity is $O(1)$ because as $\Delta t \to 0$, then $x_{p+1} \to L$ and $\bar{v}_{p+\frac{1}{2}} \to -v_{p+\frac{1}{2}}$. Finally, the v^2 approximation in Eqs. (8) and (9) introduces an error with $O\left((\Delta t)^2\right)$, which then is the lowest-order error of Eq. (A.11); hence, δ is $O(\Delta t)$. If terms are neglected with $O\left((\Delta t)^2\right)$ or greater, then the second-order approximation for δ becomes

$$\delta = \frac{2a}{v_{p+\frac{1}{2}}}(x_{p+1} - L) - a\Delta t. \tag{A.12}$$

Observe that for zero electric field at the surface, then $a=0$, and so $\bar{v}_{p+\frac{1}{2}}=-v_{p+\frac{1}{2}}$.

The maximum boundary penetration, $x_{p+1}-L=v_{p+\frac{1}{2}}\Delta t$, specifies δ at $+a\Delta t$. Minimum penetration, $x_{p+1}=L$, generates the smallest correction with $\delta=-a\Delta t$. Because the value of x_{p+1} is equally probable across the range from L to $L+v_{p+\frac{1}{2}}\Delta t$, the average value of δ after many reflections is zero. On the other hand, the correction δ generates a spread in velocities of the reflected ions. Consequently, if a substantial electric field develops at the boundary and use only simple reflection is used, the reflected ion flux would be erroneously cooled.

For a low temperature plasma, the boundary may absorb at most 20% of the incident particle energy. The specific fraction depends on the mass ratio of the incident particle and boundary target as discussed in Sec. I A of this paper. For this example then the ratio of reflected/incident ion velocity is 0.9, so that, with the above algorithm, the new reflected velocity is

$$\bar{v}_{p+\frac{1}{2}} = -0.9\, v_{p+\frac{1}{2}} + \delta. \qquad (A.13)$$

References

[1]R. S. Bhattacharya, W. Eckstein, and H. Verbeek, Surface Sci., **93**, 563 (1980).

[2]R. A. Langley, J. Bohdansky, W. Eckstein, P. Mioduszewski, J. Roth, E. Taglauer, E. W. Thomas, H. Verbeek, and K. L. Wilson, *Data Compendium for Plasma Surface Interactions,* Nucl. Fusion, special issue (1984).

[3]D. Heifetz, D. Post, M. Petravic, J. Weisheit, and G. Bateman, J. Comput. Phys., **46**, 309 (1982).

[4]G. D. Porter, Nucl. Fusion, **22**, 1279 (1982).

[5]G. A. Emmert, R. M. Wieland, A. T. Mense, and J. N. Davidson, Phys. Fluids, **23**, 803 (1980).

[6]L. A. Schwager and C. K. Birdsall, "Collector and Source Sheaths of a Finite Ion Temperature Plasma," ERL Memo M88/23, Univ. of Calif., April13, 1988.

[7]J. R. Lamarsh, *Introduction to Nuclear Engineering*, (Addison-Wesley, Reading, Massachusetts, 1983) p.59.

[8]D. Bohm, in *Characteristics of Electrical Discharges in Magnetic Fields*, edited by A. Guthrie and R. K. Wakerling (McGraw-Hill, New York, 1949).

[9]J. N. Brooks, Report No. ANL/FPP/TM-142, Argonne National Laboratory, Argonne, Illinois (1981).

[10]C. K. Birdsall and A. B. Langdon, *Plasma Physics via Computer Simulation*, (McGraw-Hill, New York, 1985).

[11]W. S. Lawson, "PDW1 User's Manual", Memo No. UCB/ERL M84/37, Electronics Research Laboratory, University of California, Berkeley, California (1984).

[12]J. F. Botha and G. F. Pinder, *Fundamental Concepts in the Numerical Solution of Differential Equations*, (Wiley, New York, 1983).

Variable List

Symbol	Name
ϕ_P	Source sheath potential drop
ϕ_C	Collector potential
F_α	Particle flux
ζ	Reflected/primary ion flux ratio
α	Reflected/primary ion velocity ratio
$T_{S\alpha}$	Source temperature
τ	Primary ion/electron source temperature ratio
M	Ion mass
m	Electron mass
μ	Electron/ion mass ratio
x	Spatial position
L	System length
$V_{M\alpha}$	Cut-off velocity
f_α	Velocity distribution function
v	Velocity
$N_{S\alpha}$	Source density
ψ	Normalized potential
N_α	Particle density
$\langle V_\alpha \rangle$	Drift velocity

T_α Temperature . . . . . .

Q_α Kinetic energy flux . . . . . .

H_α Heat flux . . . . . .

F Reference particle flux . . . . . .

δ_α Energy transmission factor . . . . . .

δ_T Total energy transmission factor . . . . . .

n_∞ Electron plasma density (used for $\tau \ll 1$) . . . . . .

n_α Particle density (used for $\tau \ll 1$) . . . . . .

T Electron plasma temperature (used for $\tau \ll 1$) . . . . . .

$\mathcal{E}$ Cold ion kinetic energy at the sheath edge . . . . . .

ϕ_F Potential drop across the collector sheath . . . . . .

W Primary ion mean kinetic energy . . . . . .

$V_{t\alpha}$ Source thermal velocity . . . . . .

The subscript α refers to primary ions i, reflected ions r, or electrons e.

The above is a list of only frequently referenced variables.